EVALUATING NEW APPROACHES TO MEASURE AND MAP SOIL MOISTURE SPATIAL VARIABILITY

By

JINGNUO DONG

Bachelor of Science in Resource and Environmental Science

China Agricultural University

Beijing, China

2010

Submitted to the Faculty of the
Graduate College of the
Oklahoma State University
in partial fulfillment of
the requirements for
the Degree of
MASTER OF SCIENCE
May, 2013

EVALUATING NEW APPROACHES TO MEASURE

AND MAP SOIL MOISTURE SPATIAL VARIABILITY

Thesis Approved:

Dr. Tyson Ochsner

Thesis Adviser

Dr. Brian Carter

Dr. Chris Zou

Dr. Michael Cosh

ACKNOWLEDGEMENTS

I would love to express my deep gratitude to my advisor Dr. Tyson Ochsner for his great help and patience through the process of writing this thesis, and all his efforts in teaching and advising me in the past three years.

I would love to thank Dr. Michael Cosh who provided a lot of help in project funding and devices, and Dr. Marek Zreda who provided support and help in the COSMOS project.

I would love to thank my committee members Dr. Michael Cosh, Dr. Chris Zou and Dr. Brian Carter. All of them provided great comments and suggestions on this thesis.

I am thankful to Justin Wehmeyer, Yohannes Yimam, Jordan Beehler, Navneet Bilga and Sam Wallace for their great help with the field experiment. I also would like to thank Bethany Scott and Dr. Xiuli Xin for their support through the process of coding and writing.

I would love to thank my friend Ming Yu and Dr. Yongfang Li, and my boyfriend Qian Li.

Name: JINGNUO DONG

Date of Degree: May, 2013

Title of Study: EVALUATING NEW APPROACHES TO MEASURE AND MAP SOIL MOISTURE SPATIAL VARIABILITY

Major Field: PLANT AND SOIL SCIENCE

ABSTRACT:

Knowledge of soil moisture spatial patterns provides basic but important information in studies of hydrological processes. At the field to subwatershed scale, soil moisture spatial variability is critical to aid in hydrologic modeling, but has not been adequately studied. Two new approaches were taken to contribute to the study of soil moisture spatial variability at this scale. The Bayesian Maximum Entropy (BME) framework is a more general method than classical geostatistics and has not yet been applied to soil moisture spatial estimation. The recently developed mobile Cosmic-ray Soil Moisture Observing System (COSMOS), i.e. COSMOS rover, has a ~660 m diameter footprint which can potentially be used in field to subwatershed scale soil moisture mapping. The objectives of this research are to compare the effectiveness of BME versus ordinary kriging (OK) for spatial prediction of soil moisture at the field scale, and to calibrate and validate a COSMOS rover for mapping 0 – 5 cm soil moisture at spatial scales suitable for evaluating satellite-based soil moisture estimates. High resolution aerial photography was incorporated into the soil moisture spatial prediction using the BME method. Soil moisture maps based on the BME and the OK frameworks were cross-validated and compared. The BME method showed only slight improvement in the soil moisture mapping accuracy compared to the OK method. The COSMOS rover was calibrated to field average soil moisture measured with impedance probes which were themselves calibrated to 0-5 cm soil moisture measured by soil sampling. The resulting rover calibration was then applied to map soil moisture around the Marena, Oklahoma In Situ Sensor Testbed (MOISST) in north central Oklahoma, USA and in the Little Washita River watershed in southwest, Oklahoma. The maps showed reasonable soil moisture patterns and a clear response to soil wetting by an intervening rainfall. The rover measured field averaged soil moisture with an RMSD of 0.039 $cm^3 cm^{-3}$ relative to the impedance probes which themselves had an RMSE of 0.031 $cm^3 cm^{-3}$ relative to soil moisture measured by soil moisture sampling. The results provide evidence that a COSMOS rover can be used effectively for near surface soil moisture mapping with acceptable accuracy.

TABLE OF CONTENTS

LIST OF TABLES

TABLES IN CHAPTER II

Table Page

LIST OF FIGURES

FIGURES IN CHAPTER II

Figure Page

FIGURES IN CHAPTER III

Figure Page

CHAPTER I

GENERAL INTRODUCTION

Knowledge of soil moisture spatial patterns provides basic but important information in studies of hydrological processes. Satellite remote sensing for soil moisture offers near global spatial coverage but it is limited to coarse spatial resolution, currently ~40^2 km^2. In situ soil moisture measurements often have small spatial support (< 1^2 m^2), so fine spatial resolution is possible but spatial coverage is generally sparse. There is a significant gap between these two measurement scales, which hinders our understanding and modeling of hydrological processes at the intermediate scale (Robinson et al., 2008).

Two strategies are proposed for bridging this gap. One is upscaling point measurements to describe large spatial patterns. Kriging as a classical spatial geostatistic method, can be applied to predict soil moisture at unmeasured points. However, kriging is a linear estimator and also assumes the field is stationary, which may not be appropriate for soil moisture data. A Bayesian Maximum Entropy (BME) framework for spatial prediction has been developed which is more general than traditional geostatistics and allows incorporation of a wider range of data types. BME has proven more accurate than traditional geostatistics for spatial prediction of soil texture (D'Or et al., 2001) and soil salinity (Douaik et al., 2004). There is a need to determine if the BME framework can provide better soil moisture mapping than traditional geostatistical methods.

Another strategy to address the "scale gap" described above would be to develop a soil moisture measurement device operating between the point scale and the satellite footprint scale. Recently the Cosmic-ray Soil Moisture Observing System (COSMOS) has been developed. This nondestructive unattended soil moisture measurement is based on detection of cosmic-ray neutrons. It has a ~670 m diameter footprint (Zreda et al., 2012). The preliminary work in Hawaii (Desilets et al., 2010) showed the COSMOS can be made mobile, which creates the possibility of on the go soil moisture mapping at a scale (1 km^2 - 100 km^2) which fits the gap between satellite and in situ measurement approaches. A complete calibration and validation of the COSMOS rover for soil moisture mapping is needed.

The objectives of this research are: first to compare the effectiveness of BME versus ordinary kriging estimators for spatial prediction of soil moisture at the field scale, and second to calibrate, validate and apply the COSMOS rover for spatial mapping of soil moisture at the field to watershed scale.

REFERENCE

D'Or, D., P. Bogaert and G. Christakos. 2001. Application of the BME approach to soil texture mapping. Stoch Env Res Risk A 15: 87-100.

Douaik, A., M. van Meirvenne, T. Toth and M. Serre. 2004. Space-time mapping of soil salinity using probabilistic Bayesian Maximum Entropy. Stoch Env Res Risk A 18: 219-227.

Robinson, D.A., C.S. Campbell, J.W. Hopmans, B.K. Hornbuckle, S.B. Jones, R. Knight, F. Ogden, J. Selker and O. Wendroth. 2008. Soil moisture measurement for ecological and hydrological watershed-scale observatories: A review. Vadose Zone J 7: 358-389.

Desilets, D., M. Zreda and T.P.A. Ferre. 2010. Nature's neutron probe: Land surface hydrology at an elusive scale with cosmic rays. Water Resour Res 46.

Zreda, M., W.J. Shuttleworth, X. Zeng, C. Zweck, D. Desilets, T.E. Franz and R. Rosolem. 2012. COSMOS: the COsmic-ray Soil Moisture Observing System. Hydrol Earth Syst Sc 16: 4079-4099.

CHAPTER II

BAYESIAN MAXIMUM ENTROPY VERSUS KRIGING ESTIMATORS OF SOIL MOISTURE SPATIAL VARIABILITY

ABSTRACT

Spatial variability of soil moisture is ubiquitous but difficult to characterize and predict, since many soil moisture-dependent processes are non-linear and scale dependent. Many classical geostatistical techniques have been developed to advance the study of soil moisture spatial variability. The Bayesian Maximum Entropy (BME) framework is a more general method than classical geostatistics and has not yet been applied to soil moisture spatial estimation. The objectives of this research are to compare the effectiveness of BME and ordinary kriging (OK) methods and to produce high resolution soil moisture maps at the field scale. High resolution aerial photography was incorporated into the soil moisture spatial prediction using the BME method. Soil moisture maps based on the BME and the OK methods were cross-validated and compared. The BME method showed only slight improvement in the soil moisture mapping accuracy compared to the OK method. Nested high resolution measurements in limited areas within the study site led to more accurate soil moisture maps for the entire site for both the BME and OK method.

INTRODUCTION

The study of soil moisture spatial variability at the field scale is important to aid in modeling hydrological processes at the land surface. The spatial patterns and the space-time evolution of soil moisture are controlled by many physiographic factors – such as topography, landscape position, slope aspect, vegetation and soil properties (Robinson et al., 2008). These factors influence soil moisture conditions through hydrologic processes which also vary in space and time. For example, during a drying period, the spatial variation of soil moisture is influenced by spatial variability in vegetation type and density (Seyfried and Wilcox, 1995), since the evapotranspiration is the dominant process in the water cycle.

Soil moisture is spatially correlated under the control of multiple hydrologic processes, and this spatial structure provides the possibility of spatial prediction and mapping of soil moisture at unmeasured points. From the classical geostatistics viewpoint, soil moisture is often assumed to be a random variable and the spatial predictions are based on soil moisture measurements at nearby points and models for the covariance or semivariance of soil moisture in space (Cressie, 1993). Many studies have been done in soil moisture spatial structure analysis by using the classical geostatistics at field to watershed scale (Brocca et al., 2007, Western et al., 1998, Western et al., 2004), and some focuses on the mapping (Bardossy and Lehmann, 1998).

Our knowledge about the physical processes and controlling factors has not been fully used in spatial prediction of soil moisture. To expand upon classical geostatistics, the Bayesian Maximum Entropy (Christakos et al., 2001) framework for spatial prediction has been advanced which is more general and allows incorporation of a wider range of data types (i.e. soft data), such as intervals, probability functions, and physical laws. The BME framework has proven more efficient and accurate than traditional geostatistics for spatial prediction of soil texture (D'Or et al., 2001) and soil salinity (Bogaert and D'Or, 2002, Douaik et al., 2004). In the comparisons

between the BME and Kriging methods, all the reported mean errors of the BME method are smaller than of Kriging (Akita et al., 2012, Bogaert and D'Or, 2002, D'Or et al., 2001, Douaik et al., 2005, Douaik et al., 2004). The BME method has also been suggested as an efficient estimator when accurate data (i.e., hard data) are scarce or expensive to collect (D'Or et al., 2001). The use of soft data can compensate for the lack of hard data, but it also makes the BME method computationally more demanding. Soft data in this context refers to information such as constraint intervals, inequalities, or qualitative data (Christakos et al., 1990).

This research focuses on studying the applicability of the BME framework in soil moisture spatial prediction at the field scale. The research area is located at the Oklahoma State University Range Research Station approximately 13 km southwest of Stillwater, OK. The site is 1.6 km wide E-W and 1.2 km wide N-S (Fig. 1a). The average annual temperature is 15 °C and annual precipitation is 831 mm (Fuhlendorf and Engle, 2004). The dominant soil series is Grainola silty clay loam, which includes moderately deep, well drained soils formed in material wathered from shale of Permian age. The soil texture varies with depth and landscape position. The National Agriculture Imagery Program (NAIP) aerial photo (Fig. 1a) shows the details of the distribution of grasses, shrubs and trees. This site is used for multiple research purposes. The Marena, Oklahoma In Situ Sensor Testbed (MOISST) occupies the eastern half of the site. The Marena station of the Oklahoma Mesonet (McPherson et al., 2007) is located in the north eastern quarter of the site.

Soil moisture has significant small-scale variability at this site. Some studies suggested that the soil moisture spatial patterns and the vegetation types are dependent on each other, but their relationship cannot be characterized by a linear regression (Rodriguez-Iturbe, 2000, Rodriguez-Iturbe et al., 1999). In this study, we hypothesized that the plant and soil conditions reflected in the aerial photo contain useful information about small scale soil moisture variability, which could help to improve the spatial estimation accuracy within the BME framework. The

NAIP image was used to generate the BME soft data set since it provides the highest resolution (~1 m) data available for this site in this study. Furthermore, aerial or satellite images are among the most widely available remote sensing data in the world. If the BME framework can effectively utilize these types of data for soil moisture mapping, then the method may have extensive applications.

The objective of this study is to produce high resolution soil moisture maps by applying the BME method. The emphasis is to compare the BME and the ordinary kriging approaches in soil moisture mapping at the field to watershed scale.

MATERIALS AND METHODS

Soil Moisture Surveys

Three surface soil moisture surveys were conducted on 8/16/2011, 1/31/2012 and 6/25/2012. About 100 georeferenced point measurements of 0-6 cm volumetric soil moisture were recorded with an impedance probe (ML2x-Theta Probe, Delta-T Devices, Cambridge, UK) in each survey. The latitude and longitude coordinates for the measurements locations were selected before the field campaign and were found in the field using handheld GPS receivers with horizontal accuracy of ±5 m. The locations were chosen to make the lag (i.e. distance between pairs of locations) distribution as uniform as possible while keeping field logistics manageable. Figure 2a shows the sampling points layout for the first survey.

In the third survey, in order to facilitate more detailed study of the spatial structure of soil moisture and vegetation patterns, a nested high resolution soil moisture sampling was conducted. A 61 × 77 m area was selected for this nested high resolution sampling, which is on the edge of the forest located in the southwest quadrant of the site. Forty-nine Theta Probe measurements

were taken on a 9 × 11 m grid. In the paper, the third survey with all sampling points is named as Survey 3a, and the Survey 3b represent the same survey but without the nested high resolution sampling points. Two individual Theta Probes were used in each survey. In the third survey, three pairs of measurements were taken closely in space at the site before the survey to compare the two Theta Probes. The average absolute difference between the two Theta Probes was 0.024 cm^3 cm^{-3}.

Cluster Analysis

In this research, an aerial photo of the study area was processed to create a soft data base. A NAIP image of the study area was down loaded from the USDA Geospatial Data Gateway (http://datagateway.nrcs.usda.gov/). This image was taken in 2010 at a one-meter ground sample distance. The image is rectified in the UTM coordinate system, NAD 83. A cluster analysis was conducted to classify the aerial photo pixels based on their RGB values. Pixels in the aerial photo were partitioned into five clusters using the Matlab function "kmeans.m", which minimizes the within-cluster sums of point to-cluster-centroid distances over all clusters. A similar cluster analysis approach has been applied for mapping surface soil organic carbon based on bare soil aerial photography (Chen et al., 2000) . The measurement locations were then classified into the same clusters as the collocated pixels.

In an effort to identify pixel clusters that contained useful information about soil moisture, each cluster was evaluated by calculating its Cluster Quality Index (CQI), which was proposed to quantify the quality of a cluster,

$$CQI_j = \frac{n_j}{\sum_j n_j} \frac{N_j}{\sum_j N_j} \frac{1}{(u_j - l_j)} \tag{2.1}$$

where n_j and N_j are the number of samples and the number of pixels in the jth cluster respectively. The upper bound u_j and lower bound l_j of the jth cluster were calculated as $u_j = \max(\chi_j) + \sigma(\chi_j)$, $l_j = \min(\chi_j) - \sigma(\chi_j)$, where χ_j refers to the soil moisture sample values in the jth cluster, and the $\sigma(\chi_j)$ is the standard deviation of the χ_j. Clusters containing relatively large fractions of the measurement locations and pixels and with relatively small ranges of measured soil moisture had relatively high CQI, and were regarded as high-quality clusters. The clusters with the top three CQI rankings were chosen to generate the interval soft data base, which consisted of the upper and lower bounds of soil moisture for each cluster.

Method of BME

From the stochastic viewpoint of geostatistics, the soil moisture is assumed to be a continuous spatial random field. Soil moisture at a particular location is considered as a random variable. Observed soil moisture values are considered to be realizations of the associated random variables. In this work, the small English letter, x, denotes soil moisture as a random variable, the small Greek letter, χ, denotes a realization of x and bold letters denote vectors.

The BME framework begins with an information measure based on the Shannon information entropy (Shannon, 1948):

$$H(\mathbf{x_{map}}) = -\int \ln[f_G(\boldsymbol{\chi}_{\mathbf{map}})] f_G(\boldsymbol{\chi}_{\mathbf{map}}) d\boldsymbol{\chi}_{\mathbf{map}} \tag{2.2}$$

where $H(\cdot)$ is the differential entropy of the continuous random vector, $\mathbf{x}_{\mathbf{map}}$, $f_G(\cdot)$ is the multivariate probability density function (pdf) of $\mathbf{x}_{\mathbf{map}}$, $\boldsymbol{\chi}_{\mathbf{map}}$ represents the realizations of $\mathbf{x}_{\mathbf{map}}$. The integral is the multiple integral across all the variables in $\mathbf{x}_{\mathbf{map}}$ integrated from $-\infty$ to $+\infty$. The notation $f_G(\cdot)$ is used to denote the pdf associated with the available "general" knowledge prior to taking any specificatory knowledge into account, so this pdf is called the "prior pdf". The random vector $\mathbf{x}_{\mathbf{map}} = (\mathbf{x}_{\mathbf{hard}}, \mathbf{x}_{\mathbf{soft}}, x_k)$, in which $\mathbf{x}_{\mathbf{hard}} = (x_1, x_2, \ldots x_{m_h})$ and $\mathbf{x}_{\mathbf{soft}} = (x_{m_h+1}, x_{m_h+2}, \ldots x_m)$, so $\mathbf{x}_{\mathbf{map}}$ consists of m random variables associated with available data (hard and soft) and one random variable to be estimated, x_k.

At the prior stage, the Maximum Entropy principle (Jaynes and Bretthorst, 2003) is applied to obtain the prior pdf, $f_G(\boldsymbol{\chi}_{\mathbf{map}})$. Namely, $H(\mathbf{x}_{\mathbf{map}})$ is maximized under available constraints. These constraints can often be expressed as statistical moment equations of the form:

$$E[g_\alpha(\boldsymbol{\chi}_{\mathbf{map}})] = \int g_\alpha(\boldsymbol{\chi}_{\mathbf{map}}) f_G(\boldsymbol{\chi}_{\mathbf{map}}) d\boldsymbol{\chi}_{\mathbf{map}} \tag{2.3}$$

where $E[g_\alpha(\boldsymbol{\chi}_{\mathbf{map}})]$ is the expectation of a known constraint function, g_α. By convention, $g_0 = 1$, so $E[g_0(\boldsymbol{\chi}_{\mathbf{map}})] = 1$ leading to the normalization constraint $\int f_G(\boldsymbol{\chi}_{\mathbf{map}}) d\boldsymbol{\chi}_{\mathbf{map}} = 1$. For $\alpha = 1, \ldots, m+1$, $g_\alpha(\chi_i) = \chi_i$, so $E[g_\alpha(\chi_i)] = E[x_i]$, that is the mean of the random variable, x_i, at a point, p_i. The set of spatial coordinates corresponding to $\boldsymbol{\chi}_{\mathbf{map}}$ is defined by p_i with $i = 1,2,\ldots,m,k$. In this work we employ the covariances between the random variables constituting $\mathbf{x}_{\mathbf{map}}$ as additional constraints (D'Or et al.,2001). Thus for $\alpha = m+2, \ldots, (m+1)(m+4)/2$,

$$g_\alpha(\chi_i, \chi_j) = (\chi_i - \overline{x_i})(\chi_j - \overline{x_j}) \tag{2.4}$$

for all possible unique pairs of points i and j, and $i, j = 1,2,\ldots,m,k$. For convenience, $\overline{x_i}$ and $\overline{x_j}$ were treated equal to the mean of soil moisture of the whole domain in practice.

The method of Lagrange multipliers is used to find $f_G(\boldsymbol{\chi}_{\mathbf{map}})$ which maximizes Eq. (2.2) subject to the constraints imposed by Eq. (2.2). The result is

$$f_G(\boldsymbol{\chi}_{\mathbf{map}}) = Z^{-1} \exp\left[\sum_{\alpha=1}^{N_c} \mu_\alpha g_\alpha(\boldsymbol{\chi}_{\mathbf{map}})\right] \tag{2.5}$$

where

$$Z = \int \exp\left[\sum_{\alpha=1}^{N_c} \mu_\alpha g_\alpha(\boldsymbol{\chi}_{\mathbf{map}})\right] d\boldsymbol{\chi}_{\mathbf{map}} \tag{2.6}$$

is the partition function and μ_α are the Lagrange multipliers. Inserting Eq. (2.5) into Eq. (2.3) yields:

$$E[g_\alpha(\boldsymbol{\chi}_{\mathbf{map}})] = Z^{-1} \int g_\alpha(\boldsymbol{\chi}_{\mathbf{map}}) \exp[\sum_{\alpha=1}^{N_c} \mu_\alpha g_\alpha(\boldsymbol{\chi}_{\mathbf{map}})] d\boldsymbol{\chi}_{\mathbf{map}} \tag{2.7}$$

The solution of this system of $N_c + 1$ equations Eqs.(2.6 – 2.7) determines the values of the Lagrange multipliers, which in turn define the multivariate prior pdf Eq. (2.5).

At the posterior stage, the Baysian conditionalization principle (Christakos, 2000) is applied to integrate the specificatory knowledge (hard and soft data), leading to the posterior pdf of the variable to be estimated:

$$f_K(\chi_k) = A^{-1} \int_I f_G(\boldsymbol{\chi}_{\mathbf{map}}) d\boldsymbol{\chi}_{\mathbf{soft}} \tag{2.8}$$

where $A = \int_I f_G(\boldsymbol{\chi}_{\mathbf{hard}}, \boldsymbol{\chi}_{\mathbf{soft}}) d\boldsymbol{\chi}_{\mathbf{soft}}$ is a normalization coefficient and I refers to the domain of the soft data vector $\boldsymbol{\chi}_{\mathbf{soft}}$. The notation $f_K(\chi_k)$ denotes the pdf is based on the total knowledge, which includes both of the general knowledge and the specificatory knowledge. In our case, the soft data is expressed in terms of intervals I_i

$$\boldsymbol{\chi}_{\mathbf{soft}} = \{[\chi_{m_h+1}, \chi_{m_h+1}, \ldots, \chi_m]' : \chi_i \in I_i = [l_i, u_i]\} \tag{2.9}$$

where l_i, u_i are the lower bound and upper bound of I_i respectively. By substituting the prior pdf into Eq. (2.8), the posterior pdf is expressed as

$$f_K(\chi_k) = (AZ)^{-1} \int_I \exp\left[\sum_{\alpha=1}^{N_c} \mu_\alpha g_\alpha(\boldsymbol{\chi}_{\mathbf{map}})\right] d\boldsymbol{\chi}_{\mathbf{soft}} \tag{2.10}$$

The posterior pdf $f_K(\chi_k)$ of x_k is maximized taking the partial derivative of Eq. (2.9) with respect to χ_k and setting it equal to zero, which yields the BME mode equation

$$\int \left\{ \exp\left[\sum_{\alpha=1}^{N_c} \mu_\alpha g_\alpha(\boldsymbol{\chi}_{\mathbf{map}})\right] \frac{\partial \sum_{\alpha=1}^{N_c} \mu_\alpha g_\alpha(\boldsymbol{\chi}_{\mathbf{map}})}{\partial \chi_k} \right\}_{\chi_k = \hat{\chi}_k} d\boldsymbol{\chi}_{\mathbf{soft}} = 0 \tag{2.11}$$

where $\hat{\chi}_k$ is the estimated mode of the $f_K(\chi_k)$. Most of the calculations were completed using Matlab R2012a with Matlab Mapping toolbox and BMElib version 2.0b. The main function that was used is "BMEintervalMode.m".

Method of Ordinary Kriging

A variogram model is typically used in ordinary kriging estimation, but in this research, we used a covariance model instead. This allowed a direct comparison of the OK and BME methods because the same covariance model was used in both.

Kriging interpolation method assumes the estimated value of $\hat{\chi}_k(\mathbf{p_k})$ is a linear combination of the known values of $\boldsymbol{\chi}_{\mathbf{hard}}$

$$\hat{\chi}_k(\mathbf{p_k}) = \sum_{i=1}^{m_h} \lambda_i \chi_i(\mathbf{p_i}) \tag{2.12}$$

where λ_i are the weighting factors chosen so that

$$\sum_{i=1}^{m_h} \lambda_i = 1 \tag{2.13}$$

The weighting factors are determined to minimize the variance $[\mathbf{x_i}(\mathbf{p_i}) - \hat{\chi}_k(\mathbf{p_k})]^2$, which can be written as the expression below (Eq. 14),

$$C(\mathbf{0}) + \sum_{i=1}^{m_h}\sum_{j=1}^{m_h} \lambda_i \lambda_j C(\mathbf{p_i} - \mathbf{p_j}) - 2\sum_{i=1}^{m_h} \lambda_i C(\mathbf{p_k} - \mathbf{p_i}) - 2\beta(\sum_{i=1}^{m_h} \lambda_i - 1) \tag{2.14}$$

where λ and β are the Lagrangian multipliers, $C(\cdot)$ is the covariance which is determined from the covariogram (Cressie, 1993). The minimum of the variance can be achieved by taking derivatives of Eq. (2.14) with respect to $\lambda_1, \lambda_2, \ldots, \lambda_{m_h}$ and β. The values of the weighting factors (Lagrangian multipliers as well) can thus be calculated.

The covariance $C(\cdot)$ in Eq. (2.14) refers to the isotropic covariance model which was established to fit the covariance estimated from the measured soil moisture values, i.e. experimental covariogram (Eq. 2.15)

$$C(|\mathbf{h}|) = \frac{1}{N(|\mathbf{h}|)} \sum_{i=1}^{N(|\mathbf{h}|)} [\chi_i(\mathbf{p_i}) - \bar{x}][\chi_i(\mathbf{p_i} + \mathbf{h}) - \bar{x}] \qquad (2.15)$$

where $N(|\mathbf{h}|)$ is the number of samples at the lag distance $|\mathbf{h}|$. Soil moisture maps were generated by estimating a series of $\hat{\chi}_k(\mathbf{p_k})$.

The damped cosine (or damped oscillation) covariance model $C(h) = \exp(-\frac{h}{\tau})\cos(\omega h)$ where $\tau \leq 1/\omega$ in $\mathbb{R}^2$ (Bellier and Monestiez, 2010, Yaglom, 1987), was introduced here. The model was modified the then applied to fit the experimental covariograms (Eq. 2.16). Two fitting parameters are a and b in Eq. (2.16).

$$C(h) = a\exp(-\frac{\pi}{2}\frac{h}{b})\cos(\frac{\pi}{2}\frac{h}{b}) \qquad (16)$$

In Eq. (2.16), theoretically, a is equal to the variance of the measurements, since $C(0) = a$. This damped cosine model characterizes a cyclic pattern according to the definition of "cycle" (Sargent, 1987). The "length" of a cycle, or the "period" of the damped oscillation is $2\pi/\omega$, which is $4b$ in our case. Therefore, b refers one quarter of the "period" and $(b,0)$ is also where the covariogram intersects the x-axis, since $C(b) = 0$.

The covariance was estimated from the measured soil moisture values using the Matlab function "covairo.m" in the BMElib version 2.0b (Christakos et al., 2001). The fitting processes were fulfilled by Excel solver using the least square error method.

Spatial Predictions and Cross-validation Analysis

The estimation points were the vertices of a 15 × 15 m grid covering the study area. In the mapping process, a maximum of 10 hard data points within 300 m of a given estimation point

were considered for both the OK and BME method and a maximum of 10 soft data points within 300 m of the estimation point were also taken into account in the BME method.

Leave-one-out cross-validations were conducted to evaluate and compare the performance of these two methods. Hard data points were withheld one at a time and the soil moisture value at its location was then estimated using both OK and BME. The mean error (ME) and the root mean square error (RMSE) of the estimation was calculated to evaluate the model performance.

RESULTS AND DISCUSSION

Statistical Properties of the Soil Moisture Observations

The statistical characteristics are listed in Table 1. Survey 2 has the highest mean value of soil moisture and the lowest CV, which indicated it was conducted in the wettest condition and the relative variability of soil moisture was less than that observed in the other surveys. In Survey 3, both the mean and the standard deviation increased after removing the nested high resolution samples. The nested high resolution sampling was conducted in a relatively dry area of the whole domain.

Figure 2a – 2d are the covariograms (covariance $C(h)$ as a function of the spatial lag distance h) of soil moisture for the three surveys. The experimental covariograms are plotted with dots and the model covariograms are shown with fitted curves. The fitting parameters for the covariance model and the r^2 values are listed in Table 2.

The covariograms of soil moisture exhibit the damped oscillations for Survey 1 and 3. Soil moisture values are positively correlated with small lag distances (<50 m), but this correlation decreased rapidly to negative values at around 100 - 200 m. The covariance then

oscillated about the x-axis. The amplitude of the covariance oscillation tended to zero as the lag distance increased. In Survey 1 and Survey 3a, more soil moisture measurements were collected at small lag distances than in Survey 2 (Fig. 4b and f), thus some detailed features of the covariogram with lag distance from 0 – 100 m are captured in the first and third surveys (Fig. 3a and c). The soil moisture measurements locations are shown in Fig. 4. The closely spaced soil moisture observations in Survey 1 and 3 not only influenced the covariogram at 0 – 100 m, but also influenced the covariogram at 100 – 300 m, especially at the lag distances with negative covariance. By comparing the covariograms for Survey 3a (Fig. 3c) and Survey 3b (Fig. 3d), this influence can be easily perceived.

The damped oscillation of the covariogram suggests a cycle in the soil moisture data. The period of the cycle is four times of the fitting parameter b for each survey. From Table 2, the values of b are divided into two groups - the ones with nested high resolution samples (Survey 1 and 3a) have relatively short period (~10^3 m), and the ones without nested high resolution samples (Survey 2 and 3b) have relatively long period (~10^4 m).

Cluster Analysis Results

In Figure 3, the bars indicate the fraction of aerial photo pixels within each cluster relative to the total number of pixels. Soil moisture observations within each cluster are plotted as circles, and the circle colors correspond to the colors in Figure 1b. The CQI values are plotted as X's and were scaled with the largest value set to one and the others scaled to the largest one. Clusters 1, 3 and 4 were selected to generate the soft data base, which resulted in that more than 80% of the pixels being used in the spatial prediction process. The upper and lower bounds for soil moisture in cluster 1, 3 and 4 are given for each survey in Table 3.

The results of the cluster analysis of the aerial photo were relatively uninformative compared to soft data used in previous studies (Bogaert and D'Or, 2002, D'Or et al., 2001) in which incorporation of soft data through the BME frame work led to improved map quality. As Fig. 2 shows, for each cluster, the difference between the upper and the lower bounds was large (about 15% - 20%). There was also near complete overlaps between intervals for the selected clusters. In contrast, in the research conducted by D'Or et al. (2001), the soft data base contained 10 narrow intervals without any overlaps between them. The relatively wide intervals and substantial overlap between intervals in this study made the soft data less informative for spatial prediction in the BME framework.

Soil Moisture Maps

The resulting soil moisture maps for each survey and method are shown in Fig. 4 to allow visual comparisons. In the maps, the soil moisture patterns are mainly controlled by the hard data with few differences between the two methods. The soil moisture maps in the right column always have similar patterns with the corresponding maps in the left column (BME). It has been shown that the BME mode estimates coincide with OK estimates when soft data are absent and the general knowledge is constrained to the mean and covariance (Christakos et al., 2001). In this study, the soft data were relatively uninformative and the patterns in the BME maps are primarily reflections of the hard data similar to the patterns in the OK maps. The soil moisture maps produced by the BME method were expected to reflect some details of the soil and vegetation patterns evident in the aerial photo, but the effects of those patterns were not pronounced (Fig. 4a, c, e and g). One visible impact of the soft data was limiting the region of influence of a few exceptionally high soil moisture observations in Survey 2. In the southwest quadrant of the maps

for that survey, areas of unusually high soil moisture are evident in Fig. 2d but are less pronounced in Fig. 2c.

Cross-validation Results

The cross-validation results for the three soil moisture surveys are summarized in Table 3. The ME statistics for both the BME and OK methods were close to 0, which indicates both methods were unbiased. The RMSE statistics for the BME method were slightly lower than for the OK method. These RMSE values are relatively low given that the uncertainty of Theta Probe is ~2%, which contributed around half of the RMSE in each survey (Table 4). In previous study, the benefit of the BME method was obvious. The RMSEs of soil texture (sand, clay or silt content) were from 4% to 10% for the BME method, and 5% to 13% for the OK method (Bogaert and D'Or, 2002, D'Or et al., 2001). In our case, the RMSEs for both of the methods were low, so the benefits of BME were hard to perceive.

For surveys without nested high resolution samplings (Survey 2 and 3b), the RMSE values are higher than for the ones with nested high resolution samplings (Survey 1 and 3a). Also, RMSE for Survey 3b is 1% (vol.) higher than it for Survey 3a. The ME for Survey 2 and 3b are greater than 0.1. The results can be partly attributed to covariogram model fitting. The modified damped cosine model was more suitable for the data with the nested high resolution samplings.

In this research, the mapping of soil moisture for the third survey was not a simple spatial prediction process, for it also included the scaling process. According toWestern et al. (2002), scaling is to distill the patterns from information at one scale and to use these to make predictions at another scale. Therefore, the effects of the small scale soil moisture measurements on the larger scale covariogram were actually a kind of scaling process.

CONCLUSION

This study represents the first known application of the BME framework for spatial prediction of soil moisture. The results demonstrate that the BME framework is applicable for soil moisture spatial estimation. The aerial photo, as soft data, provided extra information about spatial patterns of soil and vegetation which was applied in the soil moisture spatial estimation with the BME framework. However, the cluster analysis used in this research as a way of extracting and quantifying the information from the aerial photo was not effective enough to meaningfully improve the soil moisture mapping accuracy.

At the 15-m mapping resolution used in this study, the BME framework produced only slight improvement in mapping accuracy compared to OK. High resolution maps close to the resolution of the aerial photo (~1 m) could be produced using this soft data, but computational demands will increase dramatically and the impacts on the accuracy of the soil moisture maps are uncertain. At the 15-m mapping resolution, the computation time for the BME maps was about 70× greater than for the OK maps, so the small advantage in accuracy came at a relatively high computational cost. Future research could seek improvements to the BME approach for field-scale soil moisture mapping by using potentially more informative soft data such as soil texture or elevation.

REFERENCES

Akita, Y., J.C. Chen and M.L. Serre. 2012. The moving-window Bayesian maximum entropy framework: estimation of PM2.5 yearly average concentration across the contiguous United States. J Expo Sci Env Epid 22: 496-501.

Bardossy, A. and W. Lehmann. 1998. Spatial distribution of soil moisture in a small catchment. Part 1: Geostatistical analysis. J Hydrol 206: 1-15.

Bellier, E. and P. Monestiez. 2010. A spatial covariance model with a single wave effect and a finite range. Stat Probabil Lett 80: 1343-1347.

Bogaert, P. and D. D'Or. 2002. Estimating soil properties from thematic soil maps: the Bayesian maximum entropy approach. Soil Sci Soc Am J 66: 1492-1500.

Brocca, L., R. Morbidelli, F. Melone and T. Moramarco. 2007. Soil moisture spatial variability in experimental areas of central Italy. J Hydrol 333: 356-373.

Chen, F., D.E. Kissel, L.T. West and W. Adkins. 2000. Field-scale mapping of surface soil organic carbon using remotely sensed imagery. Soil Sci Soc Am J 64: 746-753.

Christakos, G. 2000. Modern spatiotemporal geostatisticsOxford University Press, Oxford ; New York.

Christakos, G., P. Bogaert and M.L. Serre. 2001. Temporal GIS : advanced functions for field-based applicationsSpringer, Berlin ; New York.

Christakos, G., P. Bogaert and M.L. Serre. 2001. Temporal GIS : advanced functions for field-based applicationsSpringer, Berlin ; New York.

Cressie, N.A.C. 1993. Statistics for spatial data. Rev. ed. Wiley, New York.

D'Or, D., P. Bogaert and G. Christakos. 2001. Application of the BME approach to soil texture mapping. Stoch Env Res Risk A 15: 87-100.

Douaik, A., M. Van Meirvenne and T. Toth. 2005. Soil salinity mapping using spatio-temporal kriging and Bayesian maximum entropy with interval soft data. Geoderma 128: 234-248.

Douaik, A., M. van Meirvenne, T. Toth and M. Serre. 2004. Space-time mapping of soil salinity using probabilistic Bayesian Maximum Entropy. Stoch Env Res Risk A 18: 219-227.

Fuhlendorf, S.D. and D.M. Engle. 2004. Application of the fire-grazing interaction to restore a shifting mosaic on tallgrass prairie. J Appl Ecol 41: 604-614.

Jaynes, E.T. and G.L. Bretthorst. 2003. Probability theory : the logic of scienceCambridge University Press, Cambridge, UK ; New York, NY.

McPherson, R.A., C.A. Fiebrich, K.C. Crawford, R.L. Elliott, J.R. Kilby, D.L. Grimsley, J.E. Martinez, J.B. Basara, B.G. Illston, D.A. Morris, K.A. Kloesel, S.J. Stadler, A.D. Melvin, A.J. Sutherland, H. Shrivastava, J.D. Carlson, J.M. Wolfinbarger, J.P. Bostic and D.B. Demko. 2007. Statewide monitoring of the mesoscale environment: A technical update on the Oklahoma Mesonet. J Atmos Ocean Tech 24: 301-321.

Robinson, D.A., C.S. Campbell, J.W. Hopmans, B.K. Hornbuckle, S.B. Jones, R. Knight, F. Ogden, J. Selker and O. Wendroth. 2008. Soil moisture measurement for ecological and hydrological watershed-scale observatories: A review. Vadose Zone J 7: 358-389.

Rodriguez-Iturbe, I. 2000. Ecohydrology: A hydrologic perspective of climate-soil-vegetation dynamics. Water Resour Res 36: 3-9.

Rodriguez-Iturbe, I., P. D'Odorico, A. Porporato and L. Ridolfi. 1999. On the spatial and temporal links between vegetation, climate, and soil moisture. Water Resour Res 35: 3709-3722.

Sargent, T.J. 1987. Macroeconomic theory. 2nd ed. Academic Press, Boston.

Seyfried, M.S. and B.P. Wilcox. 1995. Scale and the Nature of Spatial Variability - Field Examples Having Implications for Hydrologic Modeling. Water Resour Res 31: 173-184.

Shannon, C.E. 1948. A Mathematical Theory of Communication. At&T Tech J 27: 623-656.

Western, A.W., G. Bloschl and R.B. Grayson. 1998. Geostatistical characterisation of soil moisture patterns in the Tarrawarra a catchment. J Hydrol 205: 20-37.

Western, A.W., R.B. Grayson and G. Bloschl. 2002. Scaling of soil moisture: A hydrologic perspective. Annual Review of Earth and Planetary Sciences 30: 149-180.

Western, A.W., S.L. Zhou, R.B. Grayson, T.A. McMahon, G. Bloschl and D.J. Wilson. 2004. Spatial correlation of soil moisture in small catchments and its relationship to dominant spatial hydrological processes. J Hydrol 286: 113-134.

Yaglom, A.M. 1987. Correlation theory of stationary and related random functionsSpringer-Verlag, New York.

Table 1. Basic statistical properties of the 0-6 cm volumetric soil moisture data for the three surveys. N refers to the number of samples, μ refers to the mean value of the soil moisture for each survey, σ is the standard deviation, and CV is the coefficient of variation.

Survey	Date	N	μ (cm^3 cm^{-3})	σ (cm^3 cm^{-3})	CV
1	8/16/2011	95	0.141	0.0322	0.23
2	1/31/2012	84	0.271	0.0356	0.13
3a	6/25/2012	133	0.149	0.0366	0.25
3b		84	0.192	0.0455	0.24

Table 2. Parameters and statistics of the fitted covariance model.

Survey	a	b	r^2
1	6.560	98.20	0.6878
2	7.083	580.3	0.7842
3a	8.371	55.81	0.3521
3b	3.645	292.6	0.2252

Table 3. The upper and lower bounds for soil moisture in the selected clusters.

	Upper bound (cm^3 cm^{-3})			Lower bound (cm^3 cm^{-3})		
Cluster Rank	1	2	3	1	2	3
Survey 1	0.265	0.241	0.220	0.047	0.063	0.057
Survey 2	0.427	0.360	0.395	0.164	0.210	0.176
Survey 3a	0.265	0.237	0.341	0.053	0.043	0.022
Survey 3b	0.322	0.288	0.412	0.100	0.057	0.073

Table 4. Cross-validation statistics for the three surveys. Survey 3a represents the third survey with all sample points, and Survey 3b represents the third survey without the small scale measurements.

Survey	ME (vol. %)		RMSE (vol. %)	
	BME	Kriging	BME	Kriging
1	-0.0212	-0.0581	3.1102	3.1624
2	0.1835	0.1714	3.8208	3.8347
3a	-0.0748	-0.0399	3.5414	3.5906
3b	0.1043	0.1142	4.5049	4.5504

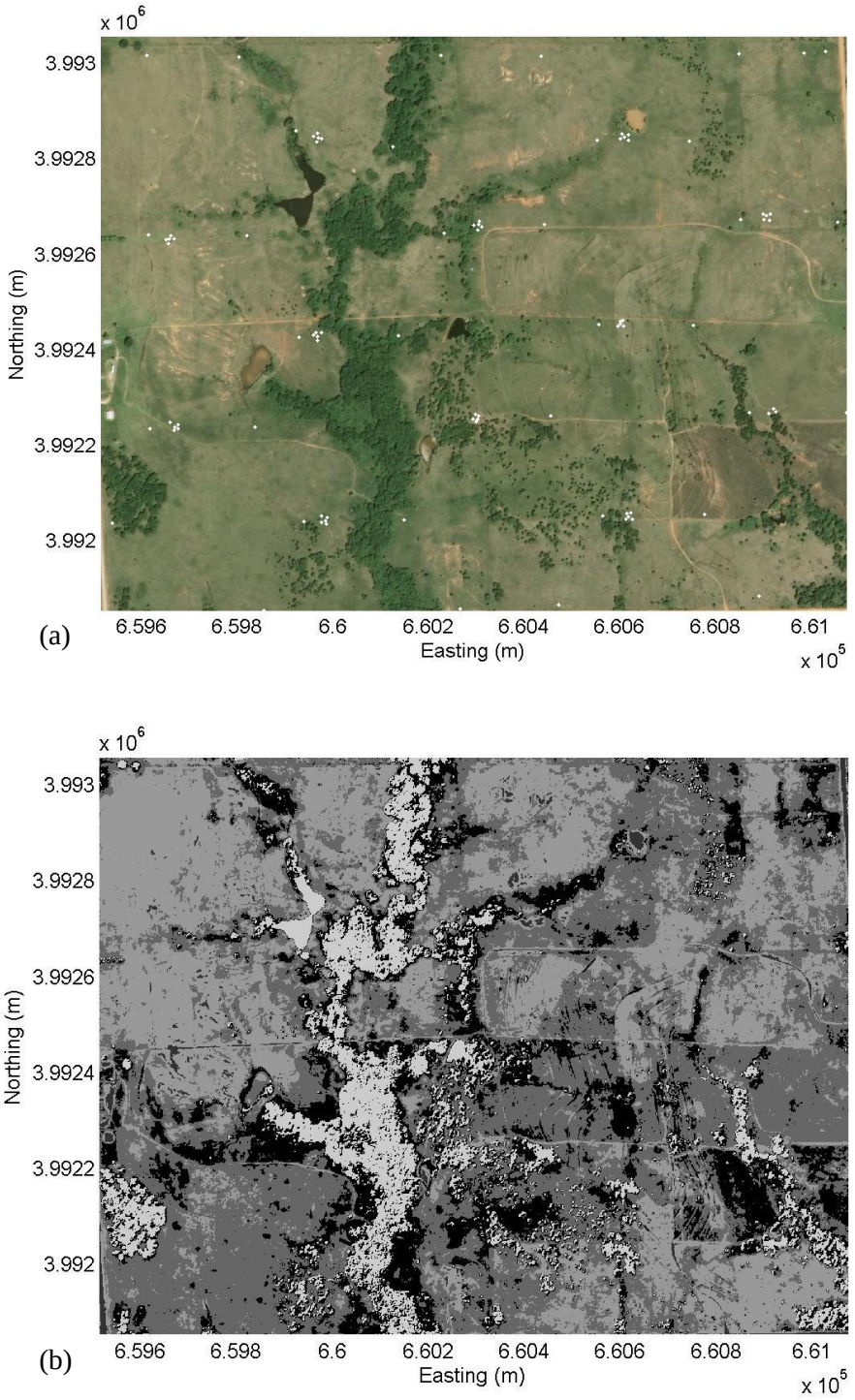

Figure 1. (a) Aerial photograph of the research area taken in 2010. Coordinates are for the UTM coordinate system, Zone 14. Hard data locations of the first survey are shown as white dots. (b) Cluster index map. Pixels of the five clusters are plotted with their cluster colors.

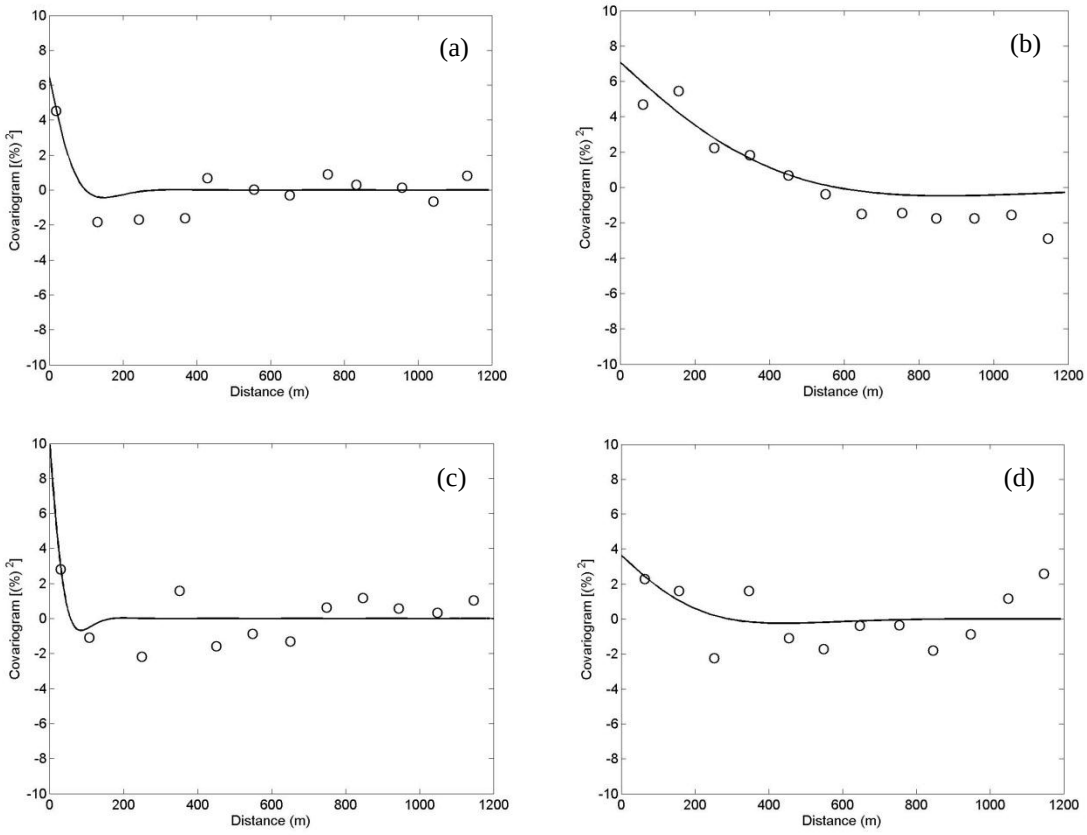

Figure 2. Covariograms of three soil moisture surveys: (a), (b) and (c) are the covariograms for the first, second and third surveys respectively; (d) is the covariogram of the third survey without the nested high resolution sampling.

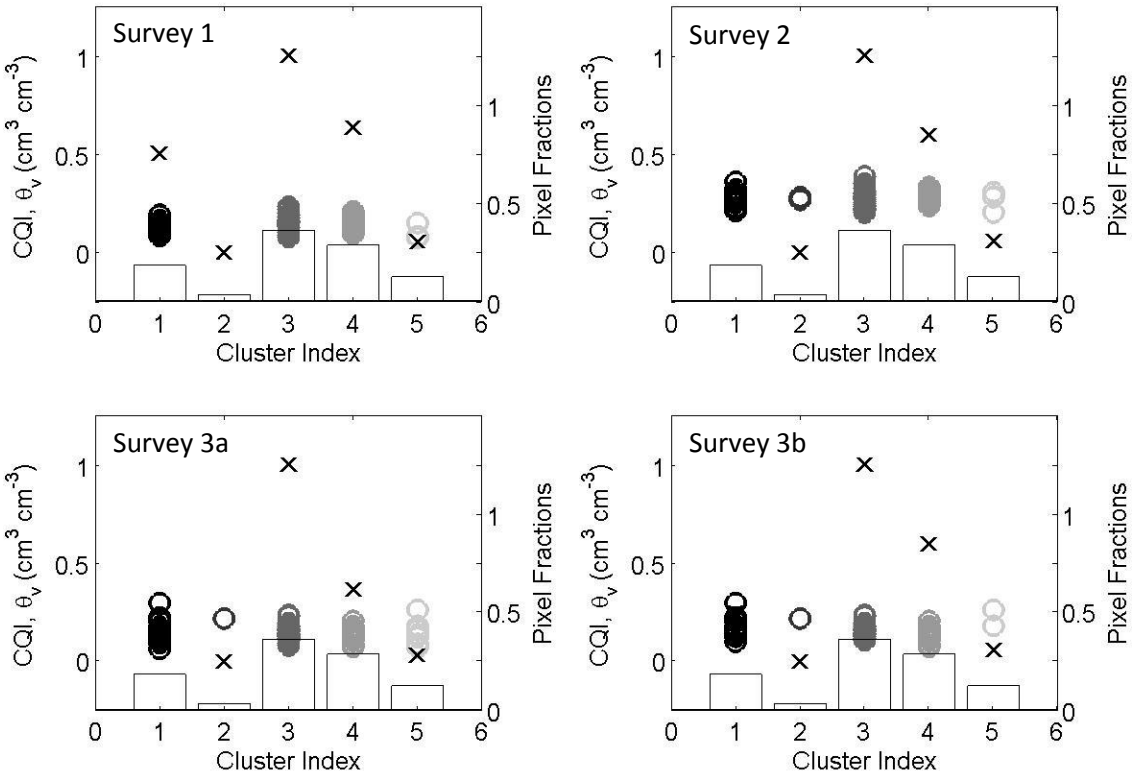

Figure 3. Cluster analysis results. The pixel fractions for the five clusters are illustrated as the white bars. Volumetric water content (θ_v) of Theta Probe measurements are plotted as circles. Crosses show the Cluster Quality Index (CQI) of each cluster.

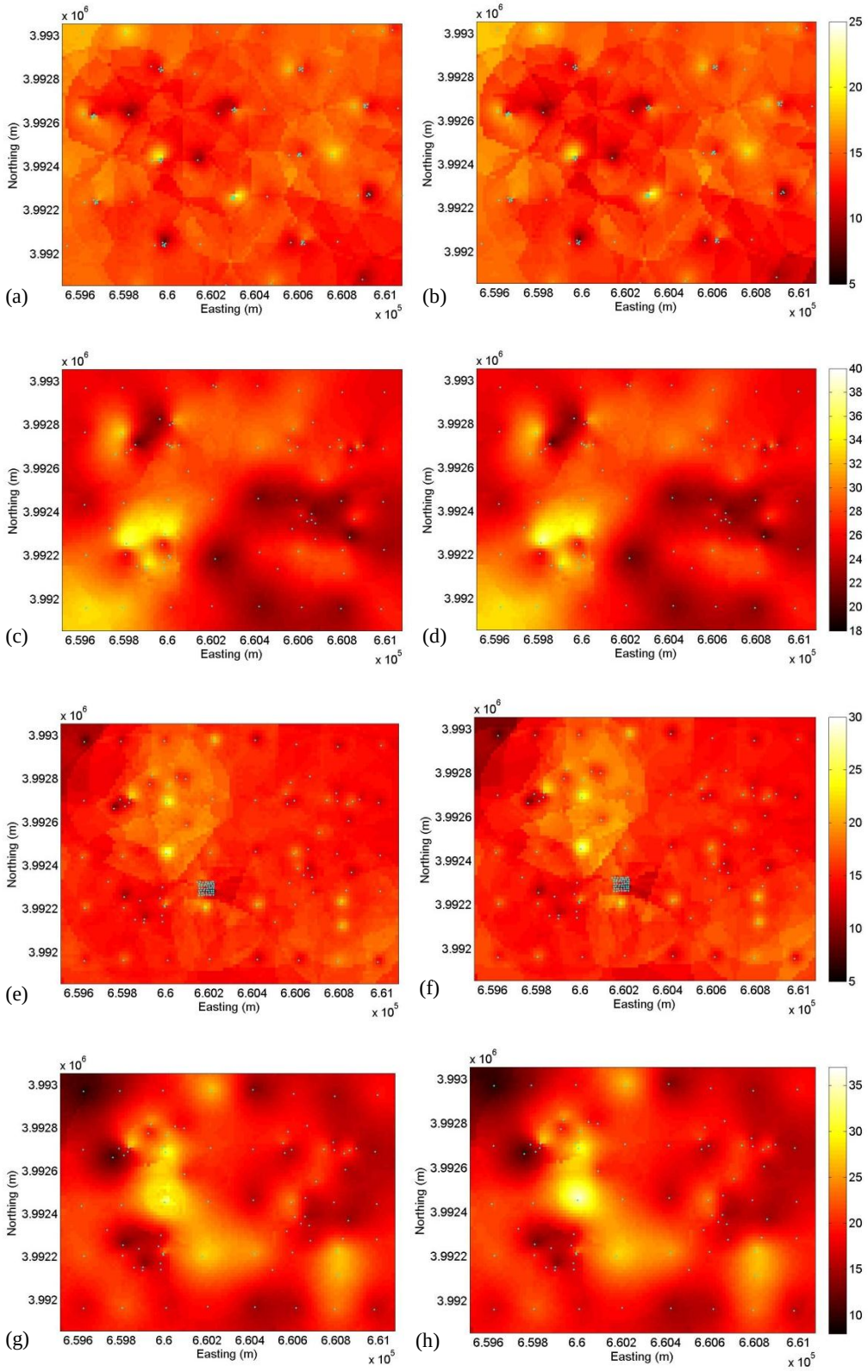

Figure 4. Soil moisture (0 – 6 cm) maps for three surveys obtained by BME mode estimation (a, c, e and g) and ordinary kriging estimation (b, d, f and h).

CHAPTER III

CALIBRATION, VALIDATION AND APPLICATION OF THE COSMOS ROVER

ABSTRACT

The recently developed Cosmic-ray Soil Moisture Observing System (COSMOS) creates unique opportunities for long-term soil moisture monitoring (stationary) and large area soil moisture mapping (mobile). One potential application of a mobile COSMOS system, i.e. COSMOS rover, is for calibration and validation of satellite remote sensing approaches for monitoring near surface soil moisture. The objectives of this research were to calibrate and validate a COSMOS rover for mapping 0-5 cm soil moisture at spatial scales suitable for evaluating satellite-based soil moisture estimates. The COSMOS rover was calibrated to field average soil moisture measured with impedance probes which were themselves calibrated to 0-5 cm volumetric soil moisture measured by soil sampling. The resulting rover calibration was then applied to map soil moisture on two dates for a 16 × 10 km region around the Marena, Oklahoma In Situ Sensor Testbed (MOISST) in north central Oklahoma, USA and on one date for a 34 × 14 km region in the Little Washita River watershed in southwest, Oklahoma. The maps showed reasonable soil moisture patterns and a clear response to soil wetting by an intervening rainfall. The rover measured field averaged soil moisture with an RMSD of 0.039 cm^3 cm^{-3} relative to the impedance probes which themselves

had an RMSE of 0.031 cm^3 cm^{-3} relative to soil moisture measured by soil moisture sampling. The regional averaged soil moisture estimates from the COSMOS rover differed by 0.0126, 0.0532, and 0.0168 cm^3 cm^{-3} from the best available independent estimates for the two MOISST surveys and the Little Washita survey, respectively. The largest discrepancy occurred when the data were collected one day after a 37-mm rainfall event when steep vertical gradients in near surface soil moisture were likely present. Overall, these results provide evidence that a COSMOS rover can be used effectively for near surface soil moisture mapping with acceptable accuracy.

INTRODUCTION

Soil moisture is a key variable influencing a wide range of agricultural, ecological, hydrological, and meteorological processes. To understand and predict soil moisture patterns at a range of spatial scales is important but challenging (Western and Bloschl, 1999). In particular, there is a gap in understanding soil moisture spatial variability for intermediate (1 – 100s km) scales due to lack of data (Western et al., 2002). To bridge this gap, the development of new techniques for soil moisture measurement at intermediate scales is needed (Robinson et al., 2008). The Cosmic-ray Soil Moisture Observation System (COSMOS) is a relatively new soil moisture measurement technique which has shown promise for measuring area-averaged soil moisture at an intermediate scale.

Cosmic rays are high-energy subatomic particles which originate in outer space (Hess et al., 1959). When the cosmic rays penetrate the atmosphere, fast neutrons are generated in the interactions of the cosmic rays with the atmospheric nuclei. Additional fast neutrons are generated as the cosmic rays interact with the land surface. As the fast neutrons travel through the air and the soil, they are moderated greatly by hydrogen near the soil surface and in the soils. Since a neutron and a hydrogen atom have similar mass, the kinetic energy loss of a fast neutron in a collision with a hydrogen atom in a collision is much greater than with other atoms. Since hydrogen in soil is mostly in the form of water, soil moisture and fast neutron intensity have a strong relationship. It has been proven that the fast neutron intensity above the land surface is inversely correlated with soil moisture (Zreda et al., 2008). This provides the theoretical basis for measuring soil moisture by fast neutron detection.

A typical stationary COSMOS probe (Hydroinnova, LLC of Albuquerque, New Mexico, USA) consists of two neutron detectors having different energy sensitivities (Desilets et al., 2010, Zreda et al., 2012). The detectors are gas (^{3}He or ^{10}B) and one of them is shielded by low-density

polyethylene, which makes the detector sensitive to fast neutrons. The neutron detectors and the associated electronics are mounted on a pole which is 1 m above the soil surface. The horizontal footprint of COSMOS is a circle with a diameter of ~660 m at sea level which depends on the atmospheric density and humidity (Zreda et al., 2008, Zreda et al., 2012). The effective measurement depth of COSMOS has a strong dependence on soil water content, which ranges from ~76 cm (0 cm^3 cm^{-3}) to ~12 cm (saturated soil) (Zreda et al., 2008). The COSMOS measurement error depends on the measured neutron count, which is a proxy for the neutron intensity. The uncertainty of the COSMOS is inversely proportional to the square root of neutron counts (Knoll, 2000). Thus, the measurement precision increases with the neutron intensity. More than 50 COSMOS stations are widely distributed in the US and abroad. This network is still being expanded and developed (Zreda et al., 2012).

Recently a COSMOS rover was developed to conduct large area soil moisture field campaigns. The COSMOS rover consists of an array of relatively large neutron counters which are mounted in a vehicle (Desilets et al., 2010). In previous studies using the COSMOS rover, soil moisture was estimated along a 35 km west-east transect in Hawaii (Desilets et al., 2010) and soil moisture was mapped for a 37 × 42 km region around the MOISST site (Zreda et al., 2011) have been conducted. However, field measurements for validation of soil moisture estimates from the rover were limited in the prior studies. Prior studies (Franz et al., 2012, Zreda et al., 2011) have suggested that cosmic ray neutron probes may be useful for calibration and validation of satellite microwave remote sensing approaches for measuring soil moisture such as the ongoing Soil Moisture Ocean Salinity mission (SMOS) or the upcoming Soil Moisture Active Passive mission (SMAP) (Entekhabi et al., 2010, Kerr et al., 2010). However, no studies have determined the accuracy with which the rover can be calibrated to 0 – 5 cm soil moisture which is the target variable for these microwave remote sensing approaches. This is shallower than the theoretically predicted effective measurement depth range for the cosmic ray neutron method. Therefore, a

more complete calibration and validation of the mobile COSMOS is needed. The objective of this study is to calibrate, validate, and apply the COSMOS rover for spatial mapping of 0 – 5 cm soil moisture at the field to watershed scale.

MATERIALS AND METHODS

Field Surveys

Field campaigns were conducted around the MOISST site on June 3, 6, and 13, 2011. The research area is located ~13 km southwest of Stillwater, OK. Five target fields were selected for rover calibration and validation, and these fields spanned ~6 km in a generally east-west transect. Each target field was 0.8 × 0.8 km. The locations of the five fields are shown in Fig. 1.

The land use of the research area is dominated by rangeland and pasture. The eastern target field was predominantly eastern redcedar, and the other four fields were grassland. Fourteen soil moisture measurements were taken distributed along two transects in each field on each survey day (0-6 cm) using impedance probes (ML2x, Theta Probe, Delta-T Devices, Cambridge, UK). Three volumetric soil samples (5 cm diameter, 0-5 cm depth) were taken per field per day for soil moisture measurement by the thermo-gravimetric method. The COSMOS rover consisted of four ^{3}He-filled proportional counters (LND, Int. and GE, Inc.) which were shielded by 2.5 cm thick polyethylene. Neutron pulse modules (Q-NPM-1000, Questa Instruments, LLC) are connected to the counters and monitor the neutron counts and send the number of counts to a data logger (Q-DL-2100, Questa Instruments, LLC). A barometric pressure sensor and a GPS receiver are integrated with the rover. Data are stored in the data logger and a removable SD card. The COSMOS rover measurements were collected at each target field with the rover sitting stationary in the field for ~36 min while the soil moisture samples were being taken. After the target field measurements on each survey day, a roving survey was completed for

the surrounding region. The roving paths are shown in Fig. 1. The yellow dots showed the small survey (13 × 5 km) which was conducted on June 3, and the red and blue dots showed the paths of the large surveys (10 × 16 km) on June 6 and June 13 respectively.

Another field campaign was conducted on June 7, 2011 in the Little Washita River watershed which is located in southwestern Oklahoma. The land use of the study area is mainly rangeland and winter wheat cropland. Soil texture ranges from sandy and silt to clay (Cosh et al., 2006), and about the center 1/3 of the watershed is sandy textured soil. The study area (~455 km^2) covers more than 70% of the Little Washita River watershed (610 km^2) (Cosh et al., 2006). The study area and the path for the roving survey are shown in Fig. 2, along with the locations of the Micronet stations.

For all rover measurements, the fast neutron counts were totaled every minute, and the GPS coordinates and barometric pressure were recorded simultaneously. The driving speed was typically 48 km h^{-1}. In our roving measurements, two of the four detectors behaved erratically and the neutron counts collected from the two detectors were not taken into consideration.

COSMOS Rover Calibration, Validation and Spatial Estimation

The rover was calibrated to 0 – 5 cm soil moisture using data from the five target fields in the MOISST region. The Theta Probe soil moisture measurements were first calibrated using the volumetric soil samples. A linear regression model was established with volumetric soil samples and Theta Probe measurements for all five fields and for the three survey days combined.

The data from the first survey day in the MOISST region were used to calibrate neutron count rates recorded with the rover stationary inside each target field to the average calibrated

Theta Probe soil moisture for each field using the shape-defining function, which characterizes the relationship between neutron intensity and soil water content:

$$\theta = \frac{a_0}{\phi/\phi_0 - a_1} - a_2 - \theta_{lat} \tag{3.1}$$

where θ is the soil volumetric water content, θ_{lat} is the soil volumetric lattice water content, ϕ (count per minute, cpm) is the observed fast neutron intensity normalized for variations in atmospheric pressure, Lattice water is here defined as the amount of water released when soil that has been dried at 105 °C is heated to 1000 °C (Franz et al., 2012). ϕ_0 (cpm) is the neutron intensity over dry soil, and a_0, a_1 and a_2 are constants (Desilets et al., 2010). In this research, the parameters values were $a_0 = 0.0808$, $a_1 = 0.372$, $a_2 = 0.115$ (Desilets et al., 2010) and the lattice water content $\theta_{lat} = 0.072$ cm^3 cm^{-3}. Lattice water content was calculated as the product of the lattice water per unit mass of 0.052 g g^{-1} reported for the MOISST site (Zreda et al., 2012) and a bulk density of 1.38 g cm^{-3}. The ϕ_0 parameter was adjusted to produce the best fit between the field averaged Theta Probe measurements and the soil water contents predicted by Eq. (3.1) for the first MOISST survey day.

All the neutron intensities were normalized to a reference pressure of 972 mbar, the average atmospheric pressure for the first MOISST survey day, using an exponential model (Desilets and Zreda, 2003) in which the atmospheric attenuation coefficient was set to 0.0077 $mbar^{-1}$. The optimized ϕ_0 value was then used in Eq. (3.1) to estimate 0 – 5 cm soil volumetric water content from the rover for the subsequent surveys, so that the calibration results can be validated. The same rover calibration was used for the Little Washita survey as for the MOISST surveys because adequate calibration data were not available in the Little Washita region.

The ordinary kriging method was used to map fast neutron intensity and soil moisture to allow visualization of the soil moisture spatial patterns. Experimental variograms were first estimated then fitted with variogram models. The fitted variogram models were analyzed for understanding soil moisture spatial structure and also OK mapping. Given the minimum distance (~ 1600m) between the rover paths and the effective diameter (650 m) of the rover, the pixel size was set to 533 × 533 m.

All the analyses in this study were conducted using Matlab R2012a with theMatlab Mapping toolbox and the BMElib version2.0b (Christakos et al., 2001).

RESULTS AND DISCUSSION

Calibration and Validation

The Theta Probe measurements were linearly related to the water content determined by soil sampling with $r^2 = 0.909$ over the range from 0.062 to 0.38 $cm^3\ cm^{-3}$ (Fig. 3). Prior to calibration, the Theta Probe tended to underestimate the actual water content. After calibration the root mean square error (RMSE) of the Theta Probe was 0.031 $cm^3\ cm^{-3}$. The quality of this Theta Probe calibration is similar to that of prior field specific calibrations ($r^2 = 0.76$ $RMSE = 0.028$) in this region (Cosh et al., 2005). The calibration results of the neutron intensity with the field average Theta Probe soil water content for the five target fields on June 3 are shown in Fig. 4. Equation (3.1) with $\phi_0 = 187$ cpm provided soil water content estimates that closely matched the Theta Probe data with $r^2 = 0.973$ and $RMSE = 0.0050\ cm^3\ cm^{-3}$. This is the first known calibration of the rover to independent field average soil moisture data and the first calibration of a cosmic ray neutron probe with 0 – 5 cm soil moisture. The typical calibration depth is 0 - 30 cm (Franz et al., 2012). Despite the unique nature of the results in Fig. 4, the

quality of the calibration is similar to that reported by Franz et al. (2012) for a stationary cosmic ray neutron probe in Arizona ($r^2 = 0.927$ and $RMSE = 0.0095$ $cm^3\ cm^{-3}$).

The shape-defining function with the calibrated ϕ_0 was validated using the second day and third MOISST surveys, and the results are shown in Fig. 5. The calibrated soil water contents from the first MOISST survey are also plotted in this figure. A 37 mm rainfall event occurred approximately 24 hr before the third survey (June 13) providing a substantial increase in the 0 – 5 cm soil water content. The validation data indicate a linear 1:1 relationship between field average 0 – 5 cm soil water content measured with the calibrated Theta Probes and that estimated with the rover across a water content range of approximately 0.10 to 0.35 $cm^3\ cm^{-3}$. The $RMSE = 0.0336$ $cm^3\ cm^{-3}$ is larger than that reported for validation of a stationary COSMOS probe, 0.0165 $cm^3\ cm^{-3}$ (Franz et al., 2012). However the maximum soil water content in that study was $< 0.25\ cm^3\ cm^{-3}$, and the uncertainty of the cosmic ray neutron probe method is known to increase with increasing water content (Zreda et al., 2012). Note that the uncertainty in the rover field averages ($RMSE = 0.0336$) is comparable to the uncertainty in the Theta Probe measurements themselves ($RMSE = 0.031$, Fig. 3). The largest discrepancy was an apparent 0.08 $cm^3\ cm^{-3}$ underestimate of 0 – 5 cm soil water content by the rover in field 4 on June 13.

It is not possible to directly validate the regional average soil water content determined with the rover because the target fields constitute only a fraction of the region of interest. However, if the target fields are representative of the region of interest, then it is useful to compare the regional average soil water content measured by the rover with that calculated from the target fields. We can strengthen the comparison by considering only the subset of rover data collected nearest to the target fields (within ~4 km). That subset is labeled as the small rover survey in Fig. 6 while the complete surveys are labeled as large rover survey. Despite these limitations, the regional average soil moisture from the roving surveys agreed well with the Theta

Probe measurements. The standard errors (Fig. 6) of the rover surveys for the wet condition (June 13) were larger than for the dry condition (June 3 and 6). This was also reflected in Fig. 5. The increases of the error and less agreement between the Theta Probe measurements and the roving measurements could be attributed to two possible reasons. One was that less fast neutrons were detected which increases the uncertainties of the measurements. The other was that the third survey was conducted one day after a rainfall event. Soil moisture may still have been moving downward and the water may have been more concentrated near the surface. During the surveys, Theta Probes were only used to measure the soil moisture at 0-6 cm, which was shallower than the effective depth of the COSMOS rover. The COSMOS roving survey in the Little Washita River watershed agreed well with the Micronet station data. The COSMOS rover average soil water content (0 – 5 cm) was 0.063 cm^3 cm^{-3} with the standard error of 0.004 cm^3 cm^{-3}, and the average soil water content of 20 Micronet stations was 0.08 cm^3 cm^{-3} with the standard error of 0.02 cm^3 cm^{-3}.

Spatial Estimation

Two maps were made for each survey - one was the neutron intensity, the other was the soil moisture. Figures 7 and 8 show maps of the neutron intensities and soil moisture for the second and third surveys in the MOISST region. Surface soil sand content and surface soil clay content maps for the study area, created using SSURGO data, are shown in Fig. 9. Some similar patterns in the southwest quadrant can be perceived when comparing Fig. 7, 8, and 9. The surface clay content is low, and the surface sand content is high in the same vicinity (Easting ~6.58×10^5 m) where soil moisture content for both of the surveys was relatively low. This correspondence between soil moisture and soil texture patterns is physically reasonable and provides indirect evidence for the validity of the soil moisture patterns recorded with the rover.

Fig. 10 is the variogram of neutron intensity for the roving survey in the Little Washita River watershed, and Fig. 11 contains the neutron intensity map (a) and the soil moisture map (b) for this survey. The range of the variogram is 2900 m, the sill is 225 cmp^2, and the nugget is 160 cpm^2. Compared with some prior studies, the range of the soil moisture variogram was often found several hundred meters at a similar scale (Warrick and Myers, 1987), but the spacing of samples was still small (~ 100 m) compared with the COSMOS (~ 650 m) . The big support volume could be the reason why the spatial structure reflected in the variogram is larger. The soil moisture patterns shown in Fig. 11 display some similarities with the soil texture map shown in a previous study in the same region (Jackson and LeVine, 1996).

CONCLUSION

The COSMOS rover soil moisture measurements were calibrated to the surface soil moisture (0 – 5 cm) successfully with one day of data, which implies that the COSMOS rover is applicable for measuring large area surface soil moisture. The accuracy of the COSMOS rover was comparable to the mission requirements (± 0.04 $cm^3\ cm^{-3}$) (Entekhabi et al., 2010) of satellite microwave remote sensing missions like SMOS and SMAP. To achieve acceptable precision, it is essential that enough fast neutrons are collected. In the roving measurements, the neutron detectors, counting intervals, and driving speed should be adjusted to meet the required precision.

In the application of COSMOS rover for soil moisture spatial estimation, one issue is how to take best advantage of the large support volume of this instrument. One straightforward way of using COSMOS rover to map soil moisture is to "scan" the entire region of interest, which means the spacing between the roving paths would be set equal to the rover footprint. Soil moisture maps could thus be made without using geostatistical spatial estimation methods.

However, in rural areas the public road network is not generally dense enough to permit this close spacing.

REFERENCES

Christakos, G., P. Bogaert and M.L. Serre. 2001. Temporal GIS : advanced functions for field-based applicationsSpringer, Berlin ; New York.

Cosh, M.H., T.J. Jackson, R. Bindlish, J.S. Famiglietti and D. Ryu. 2005. Calibration of an impedance probe for estimation of surface soil water content over large regions. J Hydrol 311: 49-58.

Cosh, M.H., T.J. Jackson, P. Starks and G. Heathman. 2006. Temporal stability of surface soil moisture in the Little Washita River watershed and its applications in satellite soil moisture product validation. J Hydrol 323: 168-177.

Desilets, D. and M. Zreda. 2003. Spatial and temporal distribution of secondary cosmic-ray nucleon intensities and applications to in situ cosmogenic dating. Earth Planet Sc Lett 206: 21-42.

Desilets, D., M. Zreda and T.P.A. Ferre. 2010. Nature's neutron probe: Land surface hydrology at an elusive scale with cosmic rays. Water Resour Res 46.

Entekhabi, D., E.G. Njoku, P.E. O'Neill, K.H. Kellogg, W.T. Crow, W.N. Edelstein, J.K. Entin, S.D. Goodman, T.J. Jackson, J. Johnson, J. Kimball, J.R. Piepmeier, R.D. Koster, N. Martin, K.C. McDonald, M. Moghaddam, S. Moran, R. Reichle, J.C. Shi, M.W. Spencer, S.W. Thurman, L. Tsang and J. Van Zyl. 2010. The Soil Moisture Active Passive (SMAP) Mission. P Ieee 98: 704-716.

Franz, T.E., M. Zreda, R. Rosolem and T.P.A. Ferre. 2012. Field Validation of a Cosmic-Ray Neutron Sensor Using a Distributed Sensor Network. Vadose Zone J 11.

Hess, W.N., H.W. Patterson, R. Wallace and E.L. Chupp. 1959. Cosmic-Ray Neutron Energy Spectrum. Phys Rev 116: 445-457.

Jackson, T.J. and D.E. LeVine. 1996. Mapping surface soil moisture using an aircraft-based passive microwave instrument: Algorithm and example. J Hydrol 184: 85-99.

Kerr, Y.H., P. Waldteufel, J.P. Wigneron, S. Delwart, F. Cabot, J. Boutin, M.J. Escorihuela, J. Font, N. Reul, C. Gruhier, S.E. Juglea, M.R. Drinkwater, A. Hahne, M. Martin-Neira and S. Mecklenburg. 2010. The SMOS Mission: New Tool for Monitoring Key Elements of the Global Water Cycle. P Ieee 98: 666-687.

Knoll, G.F. 2000. Radiation detection and measurement. 3rd ed. Wiley, New York.

Robinson, D.A., C.S. Campbell, J.W. Hopmans, B.K. Hornbuckle, S.B. Jones, R. Knight, F. Ogden, J. Selker and O. Wendroth. 2008. Soil moisture measurement for ecological and hydrological watershed-scale observatories: A review. Vadose Zone J 7: 358-389.

Warrick, A.W. and D.E. Myers. 1987. Optimization of Sampling Locations for Variogram Calculations. Water Resour Res 23: 496-500.

Western, A.W. and G. Bloschl. 1999. On the spatial scaling of soil moisture. J Hydrol 217: 203-224.

Western, A.W., R.B. Grayson and G. Bloschl. 2002. Scaling of soil moisture: A hydrologic perspective. Annual Review of Earth and Planetary Sciences 30: 149-180.

Zreda, M., D. Desilets, T.P.A. Ferre and R.L. Scott. 2008. Measuring soil moisture content non-invasively at intermediate spatial scale using cosmic-ray neutrons. Geophysical Research Letters 35.

Zreda, M., W.J. Shuttleworth, X. Zeng, C. Zweck, D. Desilets, T.E. Franz and R. Rosolem. 2012. COSMOS: the COsmic-ray Soil Moisture Observing System. Hydrol Earth Syst Sc 16: 4079-4099.

Zreda, M., X. Zeng, J. Shuttleworth, C. Zweck, T. Ferre, T. Franz, R. Rosolem, D. Desilets, S. Desilets and W. G. 2011. Cosmic-ray neutrons, an innovative method for measuring area-average soil moisture. 21:6 - 10.

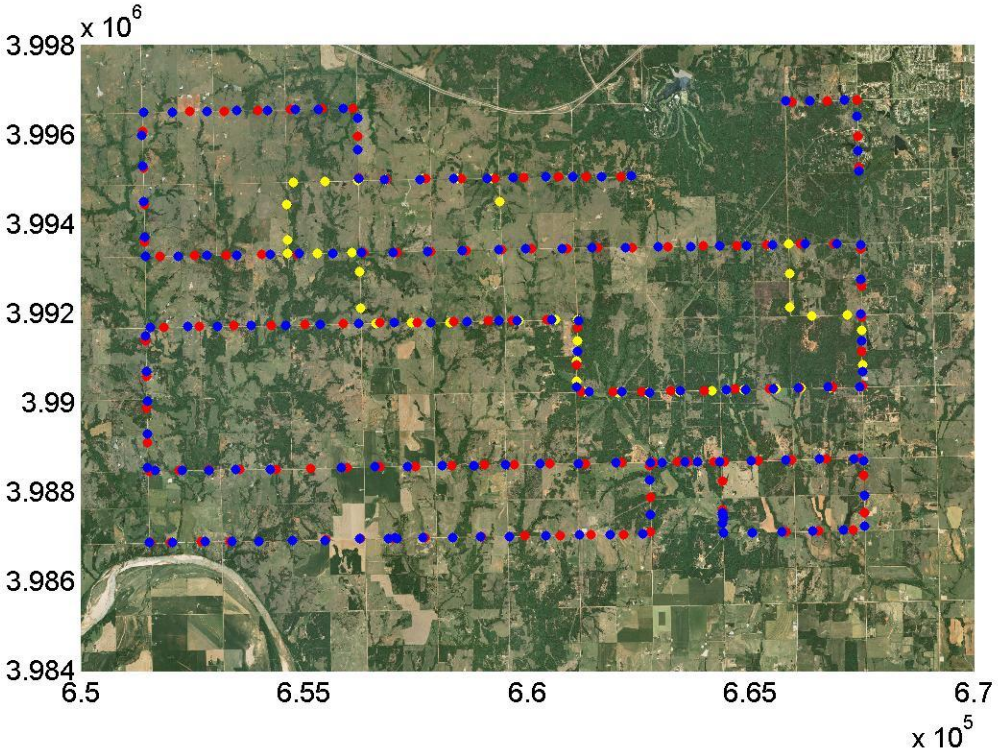

Figure 1. Aerial photo (NAIP) of the Marena, Oklahoma In Situ Sensor Testbed (MOISST) study region near Stillwater, OK. The yellow dots show the small survey on June 3, 2011, and the red and blue dots show the large surveys on June 6 and June 13 respectively.

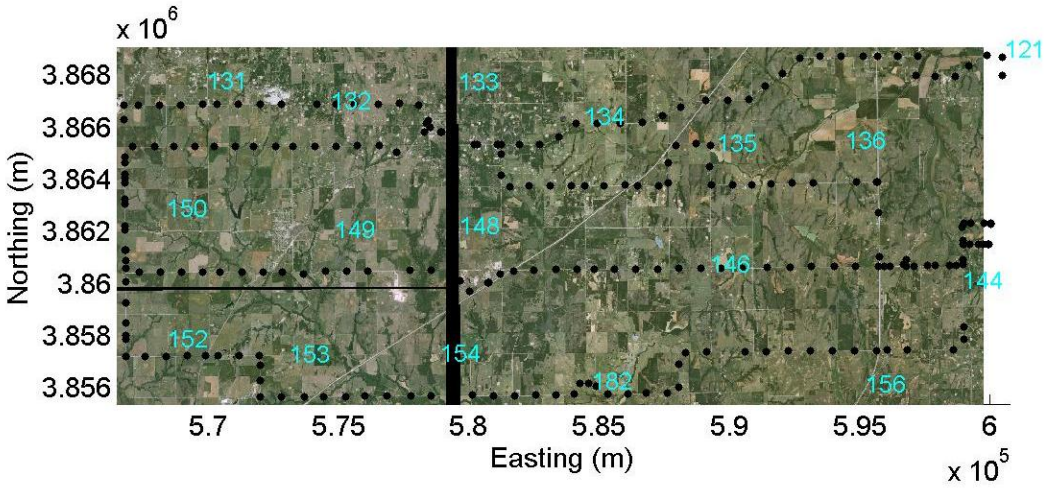

Figure 2. Aerial photo (NAIP) of the study region in the Little Washita River watershed. The black dots show roving paths.

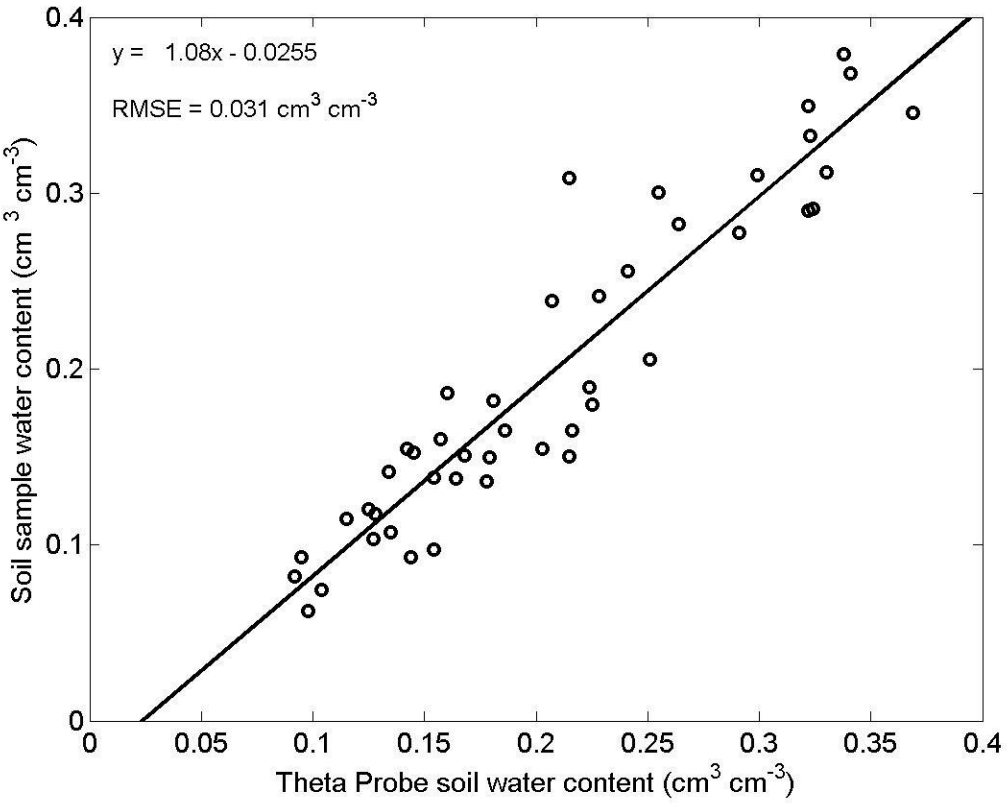

Figure 3. Volumetric soil sample water content (0 – 5 cm) vs. Theta Probe soil water content for five target fields in the MOISST region on June 3, 6, and 13, 2011.

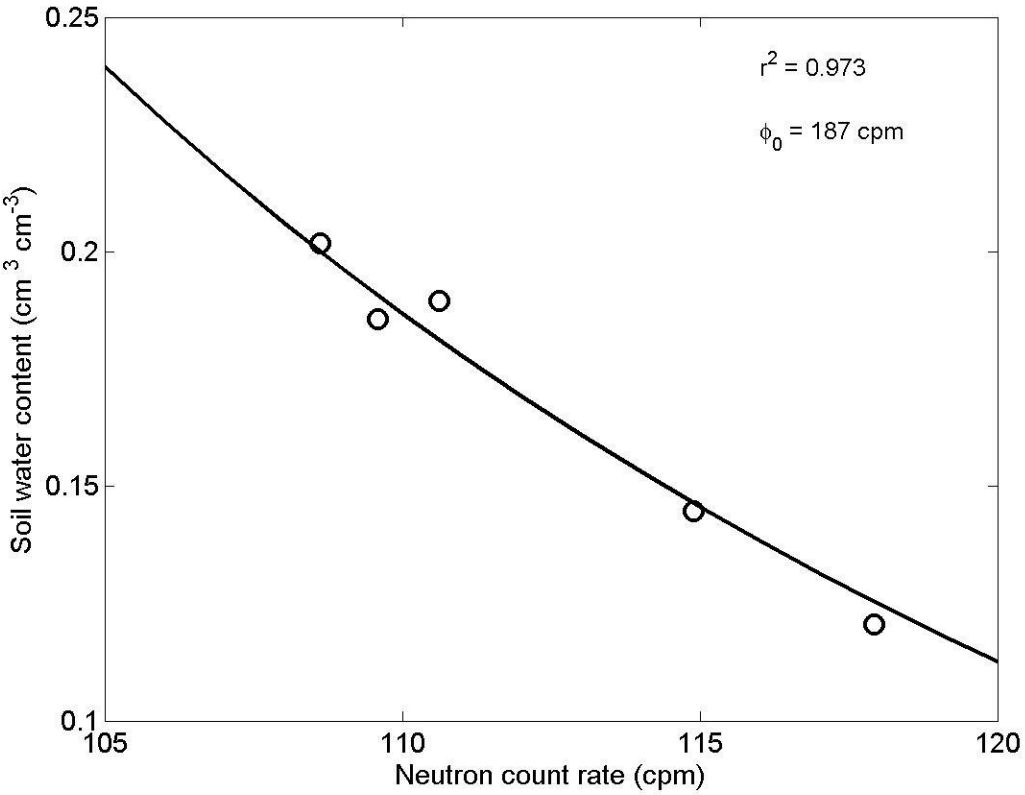

Figure 4.Calibrated shape defining function (Eq. 3.1) for the first MOISST survey (June 3) data. Circles are the averages of 14 calibrated Theta Probe soil moisture measurements in each of the five target fields. Solid line is the calibrated shape defining function.

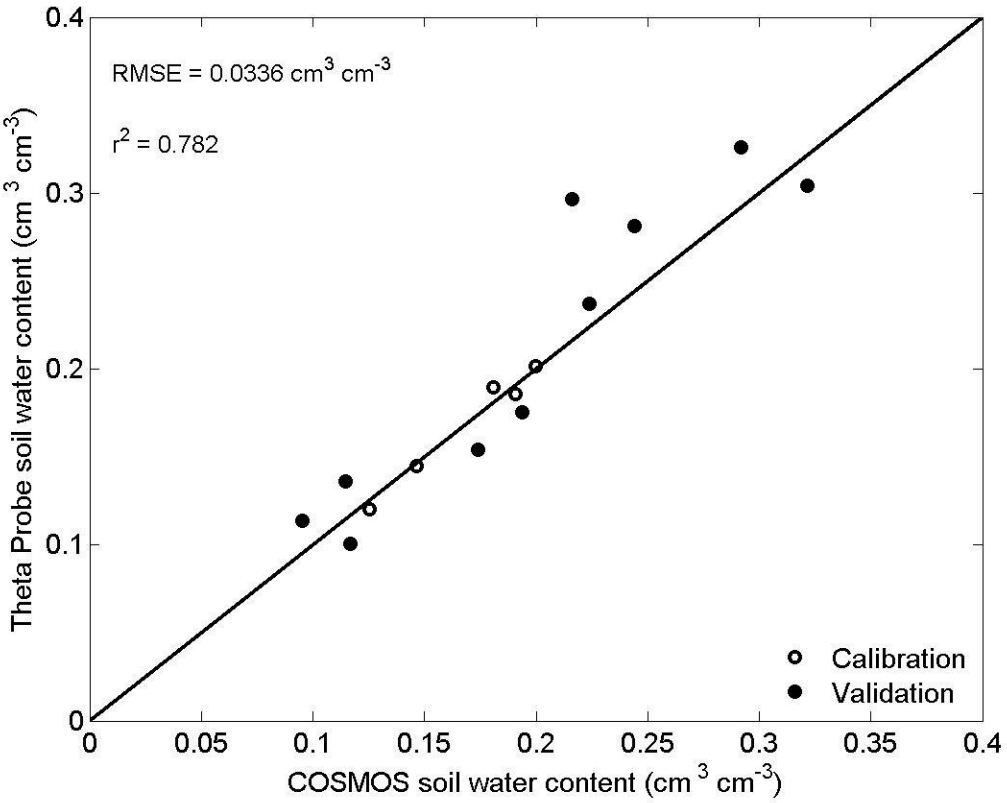

Figure 5. Field average calibrated Theta Probe soil water content vs. COSMOS rover field average soil water content (stationary) for all three MOISST region surveys. The RMSE was computed using only the validation data (June 6 and June 13).

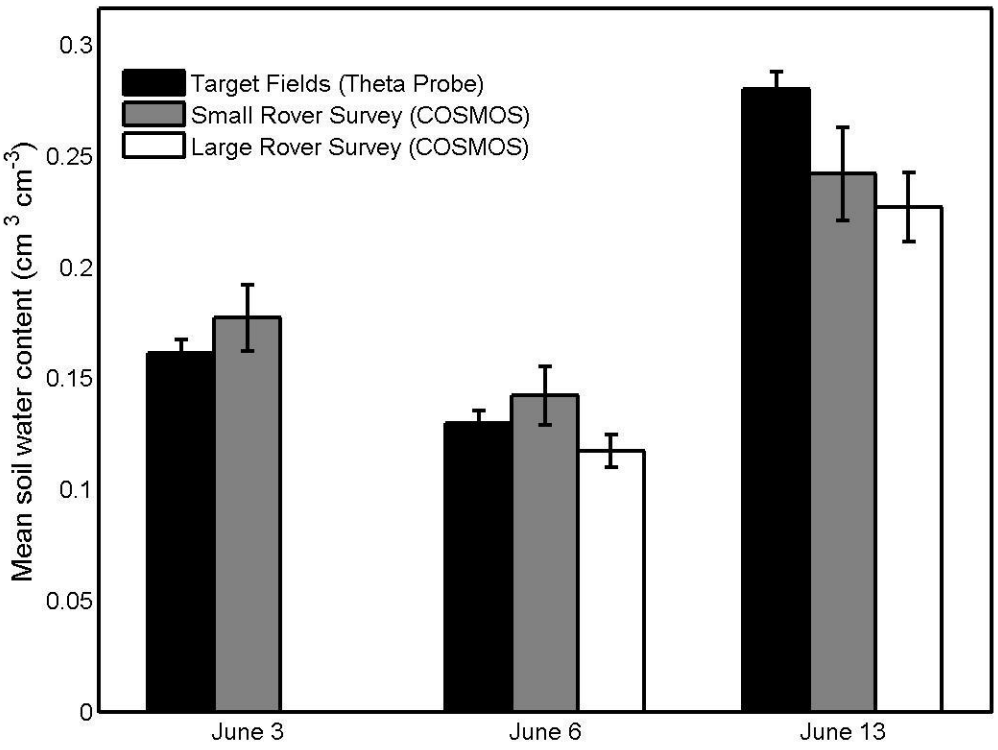

Figure 6. Comparisons of mean soil water content and standard error of the mean between Theta Probe data from the target fields and calibrated COSMOS data from the roving surveys (Small/Large Rover Survey).

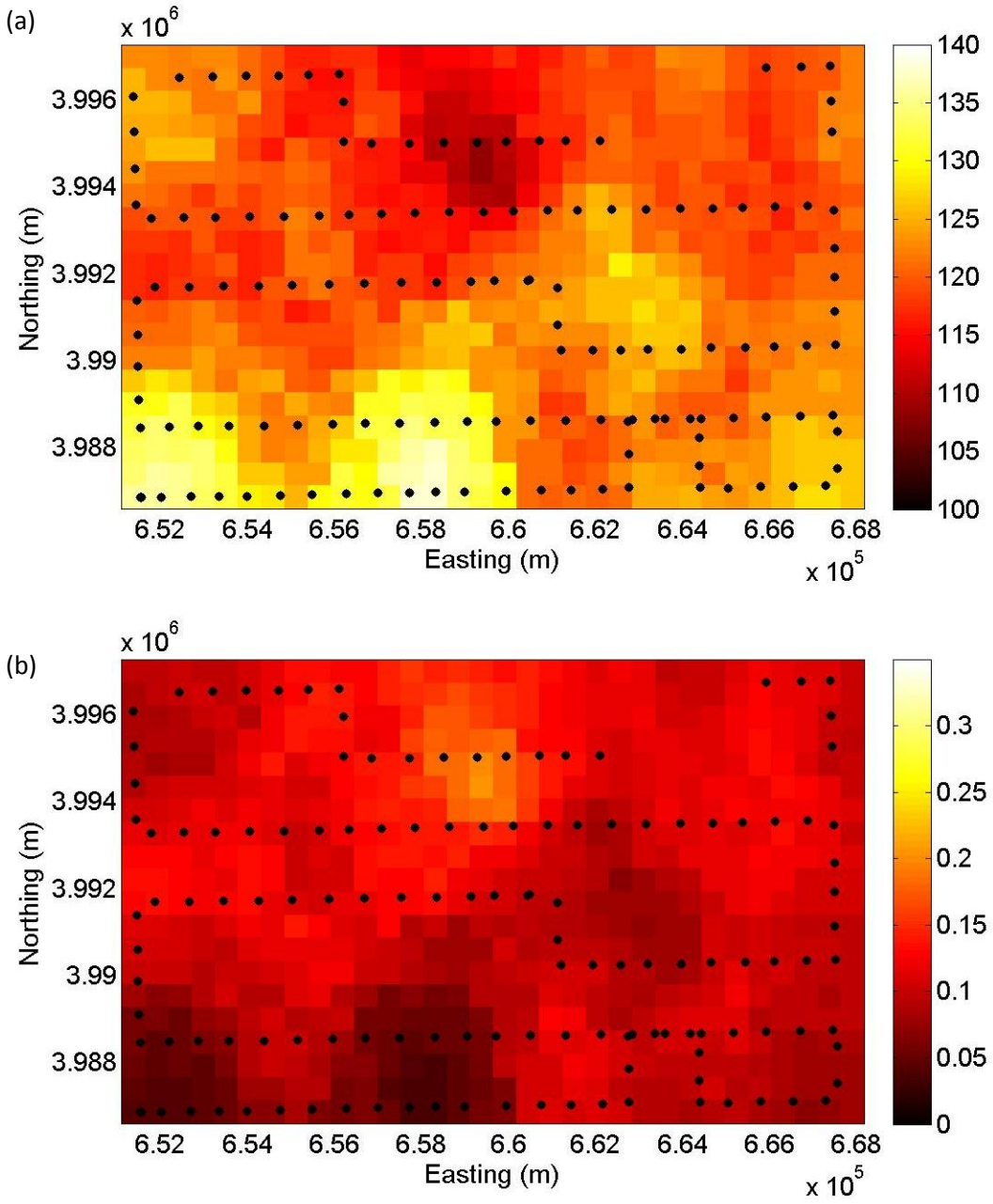

Figure 7.COSMOS rover neutron intensity (a) and soil water content estimates (b) for large surveys around the five target fields on the second survey days.

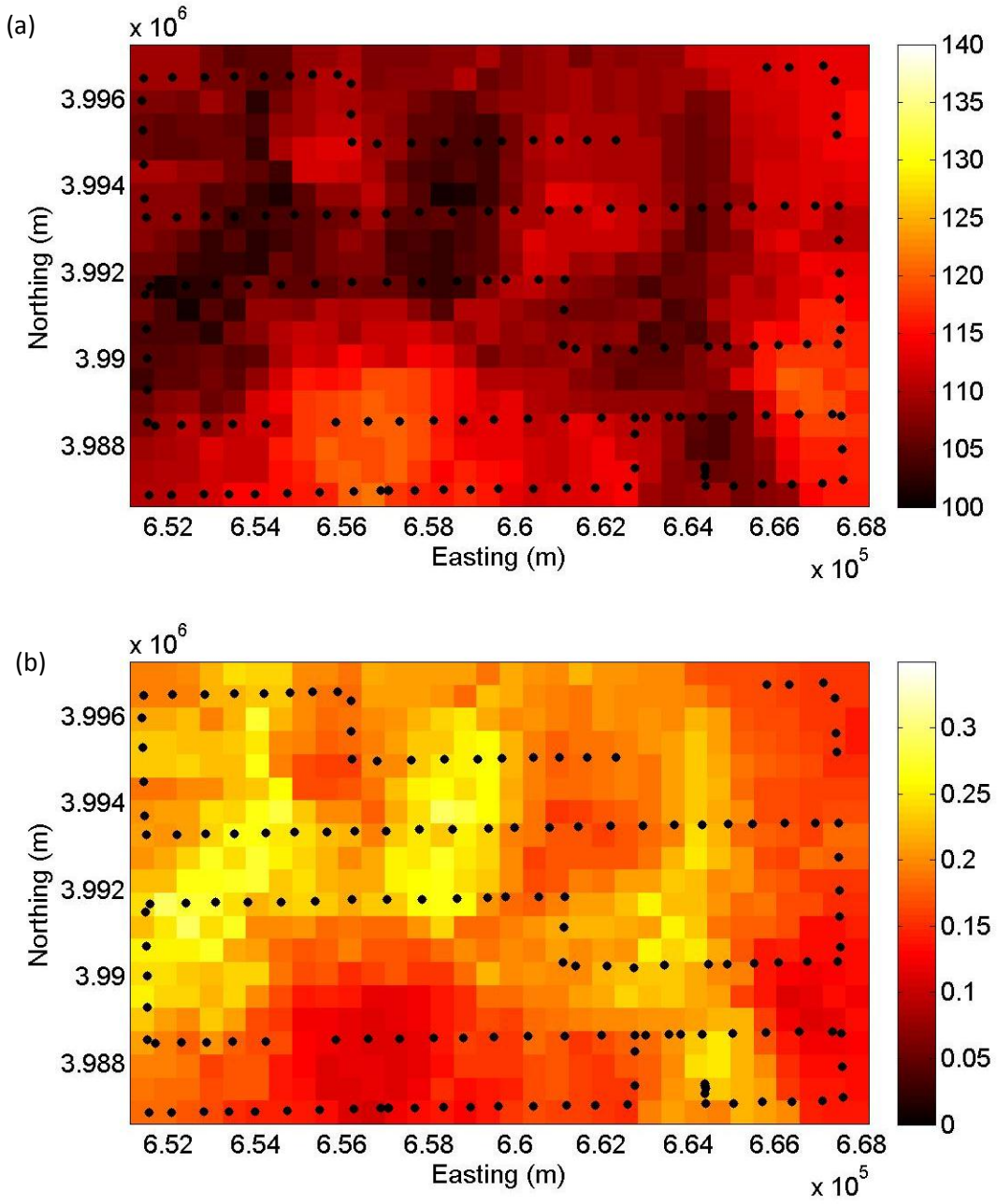

Figure 8.COSMOS rover neutron intensity (a) and soil water content estimates (b) for large surveys around the five target fields on the third survey days.

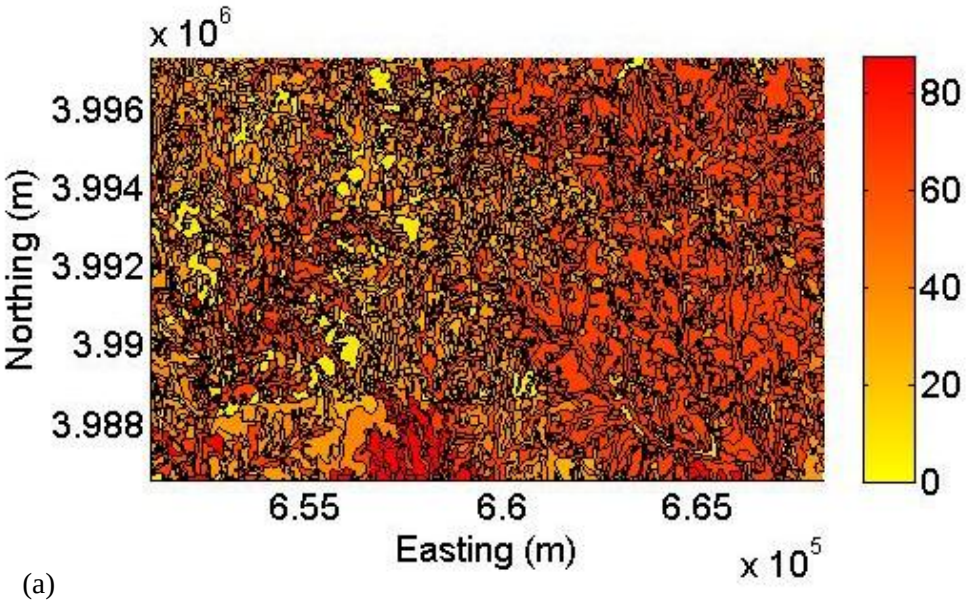

(a)

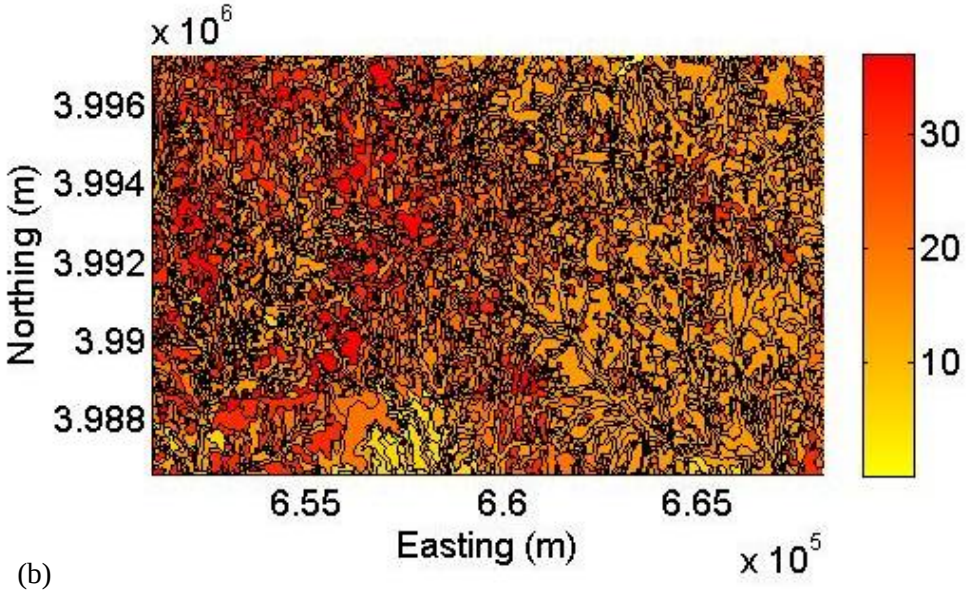

(b)

Figure 9. SSURGO estimated sand (a) and clay (b) content for the surface horizon based on the predominant soil series in each mapping unit in the MOISST region.

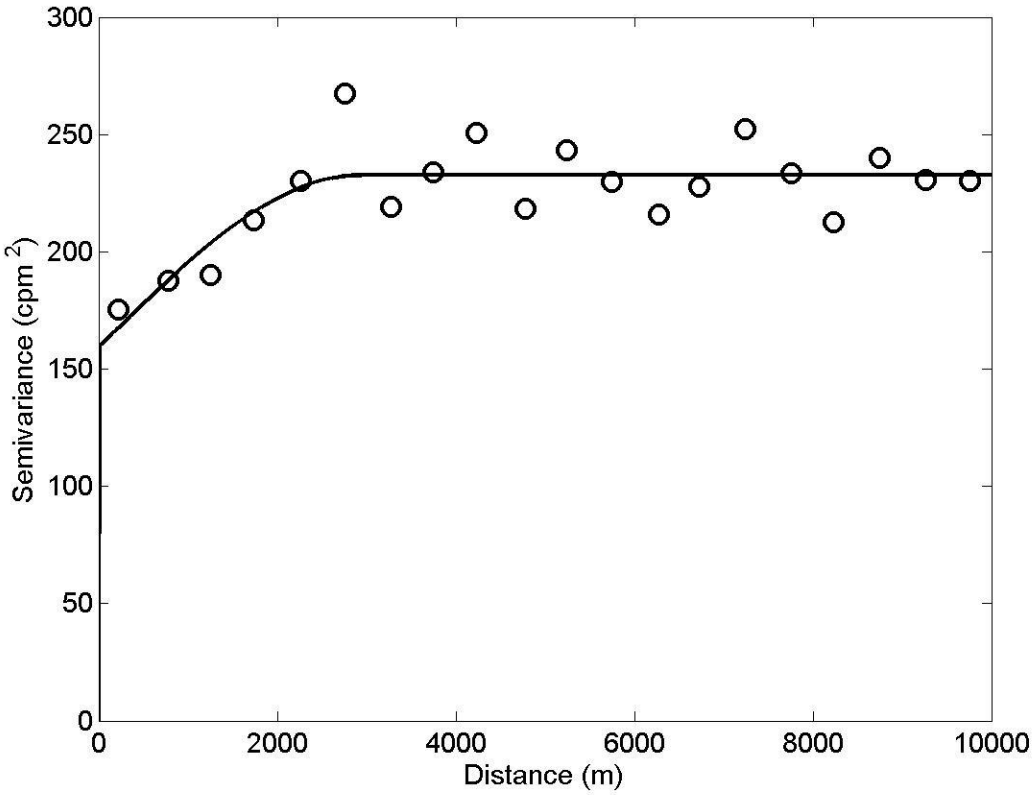

Figure 10. Neutron intensity semivariogram for the rover survey in the Little Washita River watershed on June 7, 2011.

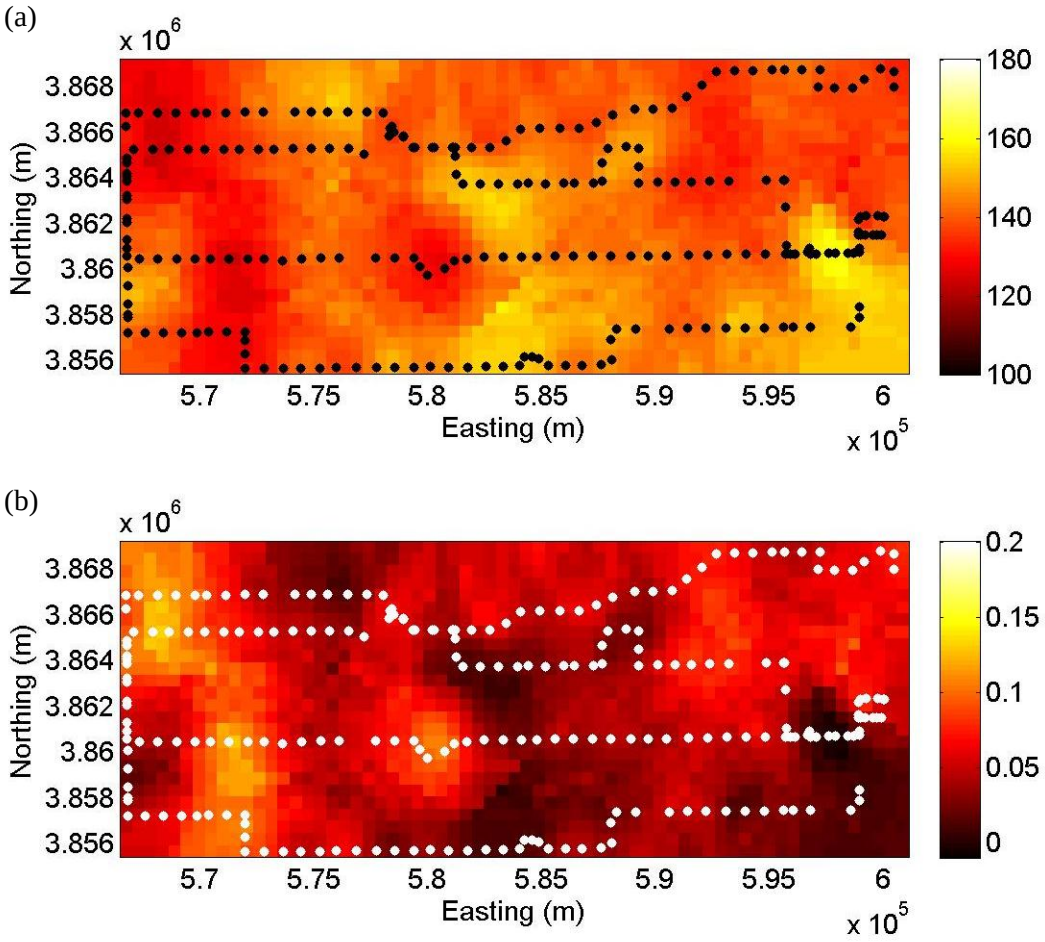

Figure 11. COSMOS rover neutron intensity (a) and 0 – 5 cm soil water content estimates (b) for the rover survey in the Little Washita River watershed on June 7, 2011.

VITA

Jingnuo Dong

Candidate for the Degree of

Master of Science

Thesis: NEW APPROACHES TO MEASURE AND MAP SOIL MOISTURE SPATIAL VARIABILITY

Major Field: Plant and Soil Sciences

Biographical:

Education:

Completed the requirements for the Master of Science in Plant and Soil Sciences at Oklahoma State University, Stillwater, Oklahoma in May, 2013.

Completed the requirements for the Bachelor of Science in Resource and Environmental Science at China Agricultural University, Beijing, China in 2010.